DECLARATION

Name: Koltsida Spyridoula-Iris

Email: iris.koltsida@gmail.com

Title of the Msc Dissertation: "Detailed numerical simulation of experiments on masonry arch bridges by using 3D FE"

Supervisor(s): Climent Molins

Year: 2011

I hereby declare that all information in this document has been obtained and presented in accordance with academic rules and ethical conduct. I also declare that, as required by these rules and conduct, I have fully cited and referenced all material and results that are not original to this work.

I hereby declare that the MSc Consortium responsible for the Advanced Masters in Structural Analysis of Monuments and Historical Constructions is allowed to store and make available electronically the present MSc Dissertation.

University: Universitat Politecnica de Catalunya

Date: 15/7/2011

Signature: _____

ACKNOWLEDGEMENTS

This work would not have been possible if there were not the people who provided me their valuable academic and personal support during these months that I have been working on this project.

First and foremost, I wish to thank my tutor, professor Climent Molins, for his collaboration and his guidance during my work. He is the person to whom I owe most of the knowledge acquired from the execution of this dissertation. I also want to express my gratitude to Oriol Arnau and Ahmed Elyamani who taught me and communicated their experience regarding the use of the finite element program DIANA 9 4.

Furthermore, I want to thank the consortium of the SAHC Master program for making it possible for me to attend this Master course by providing me a scholarship, but most of all my family who supported me economically and was always there to encourage me in difficult times.

ABSTRACT

Masonry arch bridges which are one of the oldest forms of bridges constitute a big part of the railway and roadway network of Europe. Thus the economical, functional and social value of these structures is of great importance. Moreover, because of their esthetic and technical value they constitute part of our cultural heritage which needs to be preserved.

The durability of these bridges which rises from the materials used for their construction but also from their structural behavior is remarkable. Nevertheless, they were not designed to carry the increased loads of the modern service demands. This is the reason why a big number of masonry arch bridges need to be assessed and then repaired or strengthened in order to be functional under the new necessities.

It is therefore necessary to understand the constitutive structural elements of the masonry arch bridges and how each of them contributes to the overall structural behavior of the bridge. In this way, experimental methods as well as analytical ones which can predict the behavior of these structures are needed.

Aiming to the better understanding of the structural behavior of masonry arch bridges, the Technological Laboratory of Structures of the Construction Engineering Department of UPC carried out an experimental campaign on real-scale bridges focusing mostly on the ultimate capacity and the collapse mechanisms. This thesis is dealing with one of those experiments on a semi-circular masonry bridge.

Firstly, the structural behavior as well as the current analytical methods used to evaluate the condition of masonry arch bridges are presented. Next, a summary of the design and the construction of the bridge is described as well as the instrumentation used to record the results and the loading until failure of the structure. Then, experimental results are compared with those results provided by different analytical methods.

Limit analysis using RING 2.0 was the first approach of interpreting the results. But the actual objective of this thesis is to present a finite element model able to predict the behavior of the masonry arch bridge and which can help us understand the contribution of each structural element. The results of the finite element analyses are compared with the experimental ones and some important conclusions are reached regarding the capabilities of different analytical approaches that have been used. Finally based on the gained experience some recommendations for future analytical study are given.

RESUMEN

Los puentes de arco de obra de fábrica son una de las formas más antiguas de puentes y constituyen una gran parte de la red de carreteras y ferrocarriles de Europa. Siendo así, el valor económico, funcional y social de estas estructuras de gran importancia. Por otra parte, debido a su estética y valor técnico éstos constituyen parte de nuestro patrimonio cultural que debe ser preservado.

La durabilidad de estos puentes, que no sólo proviene de los materiales utilizados para la construcción, sino también su comportamiento estructural es importante. Sin embargo, estos puentes no fueron diseñados para soportar los incrementos de cargas de las modernas demandas de tráfico. Esta es la razón por la cual un gran número de puentes de arco de obra de fábrica necesitan ser evaluados y hasta reparados o reforzados para seguir prestando servicio ante las nuevas necesidades.

Por tanto, es necesario comprender los elementos constitutivos estructurales de los puentes arco de obra de fábrica y cómo cada uno de ellos contribuye al comportamiento estructural global del puente. De esta manera son necesarios, los métodos experimentales, así como los analíticos, para predecir el comportamiento de estas estructuras.

Con el objetivo de mejorar la comprensión del comportamiento estructural de los puentes de arco de obra de fábrica, el Laboratorio Tecnológico de Estructuras de la Construcción Departamento de Ingeniería de la UPC llevó a cabo una campaña experimental a escala real de puentes enfocada principalmente en la capacidad máxima y los mecanismos de colapso. Esta tesis estudia uno de esos experimentos en un puente de arco de medio punto de obra de fábrica.

En primer lugar, se describe el comportamiento estructural, se presentan los métodos analíticos utilizados para evaluar la capacidad de puentes arco de obra de fábrica. A continuación, se resumen aspectos relativos el diseño y la construcción del puente así como los instrumentos utilizados para registrar los resultados y la carga de falla de la estructura. Los resultados experimentales se interpretan con distintos métodos analíticos.

El método de análisis límite usando el software RING 2.0 fue la primera aproximación de la interpretación de los resultados. Pero el verdadero objetivo de esta tesis es presentar un modelo de elementos finitos capaz de predecir con mayor realismo el comportamiento de los puentes de arco de obra de fábrica y que pueda ayudarnos a entender la contribución de cada elemento estructural. Los resultados de los análisis de elementos finitos son comparados con los experimentales y se llega a algunas conclusiones importantes relativas las capacidades de los distintos métodos de análisis empleados. Finalmente basados en la experiencia obtenida en este trabajo, se dan algunas recomendaciones para futuros estudios analíticos.

ΠΕΡΙΛΗΨΗ

Οι τοξοτές γέφυρες από τοιχοποιία, οι οποίες θεωρούνται ως ενας από τους πιο αρχαίους τρόπους κατασκευής γεφυρών, αποτελεί μεγάλο κομμάτι του δικτύου αυτοκινητοδρόμων και σιδηροδρόμων της Ευρώπης. Συνεπώς, η οικονομική, κοινωνική αλλα και λειτουργική αξία αυτών των κατασκευών, είναι εξέχουσας σημασίας. Επιπλέον λόγω της αισθητικής αλλα και τεχνικής αξίας τους, αποτελούν κομμάτι της πολιτιστικής μας κληρονομιάς, η διάσωση της οποίας είναι επιτακτική.

Η ανθεκτικότητα των γεφυρών αυτών στο χρόνο, η οποία είναι αποτέλεσμα όχι μόνο των υλικών κατασκευής τους αλλά και της απόκρισής τους σε φόρτιση, είναι αξιοσημείωτη. Παρόλα αυτά, δεν έχουν σχεδιαστεί για να αντέχουν τα διαρκώς αυξανόμενα φορτία των σύγχρονων απαιτήσεων κυκλοφορίας. Έτσι μεγάλος αριθμός τοξοτών γεφυρών από τοιχοποιία χρήζει αποτίμησης και εν συνεχεία αποκατάστασης και ενίσχυσης ώστε να κατασταθούν λειτουργικές υπο τις νέες συνθήκες.

Είναι λοιπόν αναγκαία η κατανόηση των συστατικών δομικών στοιχείων των τοξοτών γεφυρών και ο τρόπος που καθένα απ'αυτά συνησφέρει στην συνολική απόκριση της κατασκευής. Ετσι πειραματικές αλλα και αναλυτικές μέθοδοι οι οποίες θα είναι ικανές να προβλέπουν την δομική συμπεριφορά αυτών των γεφυρών είναι αναγκαίες.

Με σκοπό την βαθύτερη κατανόηση της απόκτισης των τοξοτών γεφυρών από τοιχοποιία, το Τεχνολογικό εργαστήριο του τμήματος Κατασκευών του UPC διεξήγαγε μια σείρα πειραμάτων σε γέφυρες αληθινής κλίμακας επικεντρώνοντας το ενδιαφέρον στο φορτίο και τους μηχανισμούς κατάρευσης. Η συγκεκριμένη διπλωματική, ασχολείται με ένα από αυτά τα πειράματα το οποίο είχε θέμα μια ημι-κυκλική γέφυρα από τοιχοποιία.

Αρχικά παρουσιάζονται η δομική συμπεριφορά αλλά και οι αναλυτικές μέθοδοι οι οποίες χρησιμοποιούνται για την αξιολόγηση της κατάστασης των τοξοτών γεφυρών από τοιχοποιία. Στην συνέχεια περιγράφεται εν περιλήψη ο σχεδιασμός και η κατασκευή της γέφυρας όπως επίσης και τα όργανα τα οποία χρησιμοποιήθηκαν για την καταγραφή των αποτελεσμάτων αλλά και η διαδικασία φόρτισης της γέφυρας μέχρι την κατάρευση. Τέλος τα πειραματικά αποτελέσματα συγκρίνονται με αυτά που προέκυψαν απο αναλυτικές μεθόδους.

Η ανάλυση οριακής αστοχίας της γέφυρας με την χρήση του προγράμματος RING 2.0 αποτελεί το πρώτο βήμα της αξιολόγησης των αποτελεσμάτων. Όμως βασικός στόχος της παρούσας διπλωματικής αποτελεί η παρουσίαση ενός μοντέλου πεπερασμένων στοιχείων, ικανό να προβλέψει την απόκριση της κατασκευής και το οποίο θα μας βοηθήσει να καταλάβουμε την συνεισφορά καθενός δομικού στοιχείου. Τα αποτελέσματα της ανάλυσης με πεπερασμένα στοιχεία συγκρίνονται με τα πειραματικά φτάνοντας σε σημαντικά συμπεράσματα σχετικά με την ικανότητα καθεμιάς από τις αναλυτικές μεθόδους που χρησιμοποιήθηκαν. Τέλος, βασισμένοι στην αποκτηθήσα γνώση, δίνουμε κάποιες συστάσεις για μελλοντική μελέτη.

TABLE OF CONTENTS

LIST OF FIGURES

LIST OF TABLES

1. INTRODUCTION

1.1 Masonry arch bridges

Hundreds of road and railway bridges all around Europe are masonry arch bridges. This typology of bridges is ancient and its durability through time, remarkable as demonstrated by many old masonry bridges which are still in operation.

Figure 1- 1 Arta bridge (Greece). Pylh Trikalon bridge (Greece). Zagori bridge (Greece)

Arch bridges are still built nowadays but in a different form. The new arch bridges are usually made of concrete or steel because of the need to span big distances and also because the use of these materials is easier and more economical.

The durability of the masonry arch bridges lies not only in their shape which provides great resistance to the structure but also in the material itself. Masonry is one of the most ancient construction techniques. The simplicity of its manufacture process and the availability of raw material (earth, clay, stone) allowed it to become the most used, ancient and widespread of construction techniques. Despite the simple construction process, it is highly durable, resistant and flexible.

The qualitative value of the masonry arch bridges is difficult to be estimated, and we can not perform a simple economic evaluation. Most of these bridges are part of our cultural heritage and the need to preserve them obvious.

The importance of strengthening and restoring this kind of structures, lies in the understanding of their structural behavior, both in service and in fatigue (as in any type of structure). In addition to the above, in most cases, these bridges were created to meet the specific needs of the time they were built, while currently are being used serving the modern traffic (increased intensity and speed of traffic). This fact increases the permanent load and most specifically there is a notable increase not only of the live load but also of the dynamic effects. This change in operating conditions is also associated with greater demands on functional quality and safety of the users.

It is clear that for a proper repair of these structures adequate analysis tools which enable the determination of the condition of the structure in order to apply a repair as simple and discrete as possible, without changing the appearance, the functionality, the way of working or the esthetics of the bridge, are needed. This applies as much to the old structures as to modern ones. But the uniqueness of the old materials against the well-known materials such as steel and concrete, and the lack of teaching on these old materials and masonry structures in structural engineering schools, have frequently led to unsuitable restorations.

1.2 Objectives of the thesis

The Department of Construction Engineering of UPC performed an experimental campaign of masonry arch bridges led by Professor Pere Roca. The bridge under study in the present thesis was designed in 2002 and its construction was performed during the academic year 2002 -2003. Its testing until collapse was held on Thursday July 10, 2003.

The main objective of this thesis is to simulate numerically the behavior of this masonry arch bridge near collapse, its ultimate capacity and its collapse mechanism.

In more detail, this dissertation aims at the following:

- Study of the structural behavior of masonry arch bridges and of the analytical methods which have been used in past or which are still in use.
- Understanding of the geometry and the material properties of the masonry arch bridge tested in the Laboratory of Structural Technology of UPC as well as of the loading procedure and the results of the experiment.
- First evaluation of the results using a limit analysis.
- Generation of different finite element models (in both 2D plane stress and 3D FE) able to reproduce the results of the experiment and able to predict the results of future full scale experiments on masonry arch bridges.
- Evaluation of the actual behavior of the soil infill.
- Evaluation of the contribution of the spandrel walls to the resistance of the structure.
- Evaluation of the contribution of the bracing system to the ultimate capacity of the bridge and to the collapse mechanism.

1.3 Contents of this Master's thesis

This dissertation is divided into six chapters. In the first chapter, we are giving a brief introduction about masonry arch bridges in general and we are also presenting the objectives to be fulfilled within this thesis.

Chapter 2 includes the basic information on the structural behavior of a masonry arch bridge and on the structural and non structural elements constituting this kind of structures. We are also describing the analytical methods which are used, or were used in the past to predict the behavior and the collapse mechanisms of masonry arch bridges.

In chapter 3, we are presenting in detail the geometry and the materials of the masonry arch bridge tested by the Laboratory of Structural Technology of UPC as well as the construction procedure, the instrumentation used to record the results of the experiment and the implementation of the test. In the last part of this chapter we can see the results of the test as well as a limit analysis of the bridge.

Chapter 4 is presenting three different plane stress finite element models of the bridge, the results from linear and nonlinear analyses and the comparison between the three which helps us to understand the influence of the soil and the bracing system to the ultimate capacity of the bridge.

In chapter 5 we are presenting the linear analysis of the three dimensional finite element model of the structure which was created to simulate the actual geometry of the structure with all of its elements.

Finally in chapter 6 the results of all the analyses are discussed and conclusions are reached regarding the capabilities of the different analytical approaches that have been used. We are also giving suggestions for further research of the subject.

2. CURRENT STATE OF KNOWELEDGE

2.1 Introduction

This chapter is intended to summarize the current knowledge on the structural behavior of masonry arch bridges as well as the evolution over the years on the structural analysis of this kind of structures.

In the first part a short description of the structural elements constituting a masonry arch bridge as well as the materials usually used in such a structure is presented. Also we are presenting the structural performance of masonry arch bridges under loading.

In the last part of the chapter we are describing the structural analysis methodologies which are used or have been used in the past for the evaluation of masonry arch bridges.

2.2 Geometry and structural behaviour of a masonry arch bridge

2.2.1 Constitutive elements of a masonry arch bridge

A masonry arch bridge is composed of structural and non structural elements. Generally the parts constituting a masonry arch bridge are shown in Figure 2-1. The structural elements are the following:

- The masonry arch. The arch is a structural element of the bridge. It can be constructed with blocks of stone wedge-shaped, generally called segments (voussoirs) or with one or more concentric rows of bricks. Generally, bridges are constructed using segments to maintain a symmetrical arrangement with respect to a central segment, which is often called key (keystone). The special nature of this slice is more aesthetic and traditional, but not structural.

  The convex surface of the arch ring is called extrados while the concave one, is called intrados.

  The structural role of the masonry arch is basically to withstand compression loads.
- Abutments. Abutment is the part of a bridge which provides resistance to horizontal and vertical forces from an arch ring. The block in each abutment on which rests the last segment or brick of the arch is called skew-back. The surface of the abutment which is also part of the arch is called springing.
- Piers. Pier is an intermediate support between adjoining arch spans.
- Spandrel walls. The walls that laterally constrain the filling over the extrados of the arch to the level of road are called spandrel walls. These walls can go on to become wings walls in the area over the supports. The wing-walls are the retaining walls of the filling in the zone of the abutments. The direction in plan of the wings should not necessarily be parallel to the axis of the road, but can be oblique or even normal to this axis.

- Filling. The term filling encompasses all the material that is located between the masonry arch barrel, the spandrel walls, the abutments and the road surface. Therefore, speaking of filling refers to a variety of materials and conditions. The filling material is usually an incoherent material (such as soil) or, in order to reduce the thrust on the walls, it may be constituted by dry stones, coarse aggregate, gravel, ballast or for more recent bridges, low resistance concrete.

  The infill material must be light and able to drain the water. This prevents an accumulation of water that would compromise the functionality of the bridge and at the same time would increase the load that the structure is called to bear. Moreover it should contribute to the repartition on the arch of the concentrated loads applied on the horizontal plane on top of it.

  For the analysis of the bridge, it is important to know the type and properties of the materials that constitute the filling, but also its degree of compaction, saturation and confinement.
- Backing. Sometimes there is some additional masonry between the arch and the filling, which is usually considered part of the filling. This is commonly presented as a backing in the area near the springing of the arch, i.e. in the transition zone between the arch and the pier or between the arch and the buttress. This is usually of a lower quality material than the rest of the brickwork, but being a bonding material does provide additional support to the structure.
- Foundation. Foundation is that part of the structure in direct contact with and transmitting loads to the ground. Foundations of masonry arch bridges have a large number of typologies and building materials. Thus, the foundation can be superficial, deep, on rock, on wooden slates, etc. Knowing the type and material with which the foundation is built and its condition, as well as the geotechnical properties of the soil is essential for the analysis of the bridge, and can be a major cause of uncertainty.

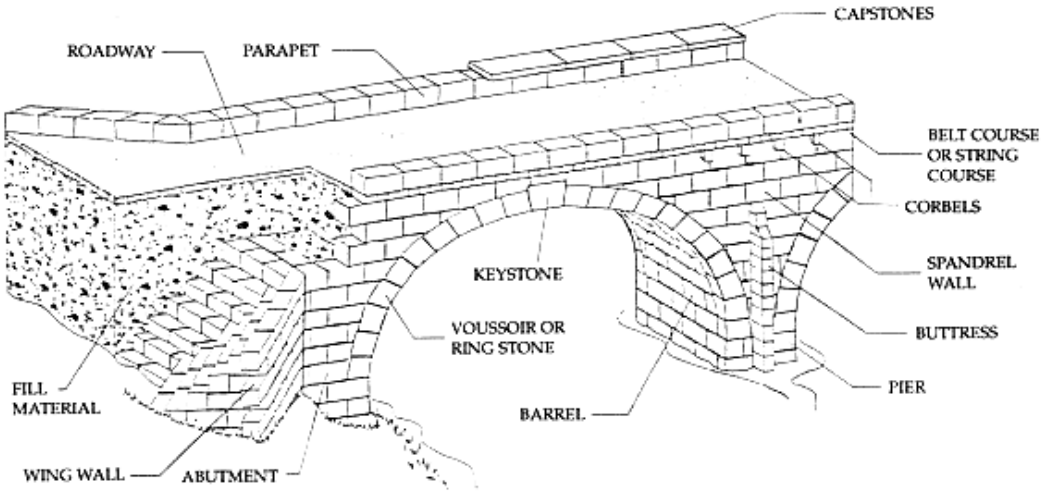

Figure 2- 1 Identification of the different parts constituting a masonry arch bridge.

The non structural elements that are met on a masonry arch bridge are the parapets and the pavement. The parapets are raised above the spandrel walls. They are an element of protection from falls for the users of the bridge while performing also an aesthetic function. Pavement on the other hand is the bound material forming footpath/verge or carriageway and includes surfacing and road bas, but excludes sub-base.

2.2.2 Structural behaviour of masonry arch bridges

An arch bridge is based on the concept of spanning an opening with a curved structural member. The arch transmits the load from the bridge deck to the abutments on both sides of the span and thus to the ground below. The arch pushes downwards and outwards against its abutments, which must be heavy and stiff enough to resist the thrust. Since the abutments transfer both horizontal and vertical forces from the bridge deck, arch bridges are used where the ground or the foundation is solid and stable. The curved arch barrel offers high resistance to bending forces.

The basic structural element of a masonry arch bridge is the arch barrel itself. Thus, the structural behavior of this kind of bridges is similar to the structural behavior of any vaulted structure. But the actual structural behavior of a masonry arch bridge is much more complex than this because of the interaction between the different structural elements as well as the different materials.

It has to be mentioned that the materials constituting the structural elements of a masonry arch bridge are characterized as being heterogeneous, anisotropic and even discontinuous. In other words all the constituents of the masonry can not withstand tensile stresses.

Another key aspect of masonry bridges is the presence of structural elements of different nature and with different behavior. Thus, the arch, the filling, the spandrel walls, the piers, the wings and the abutments interact with each other and each of them contribute in a different degree to the resistance of the structure.

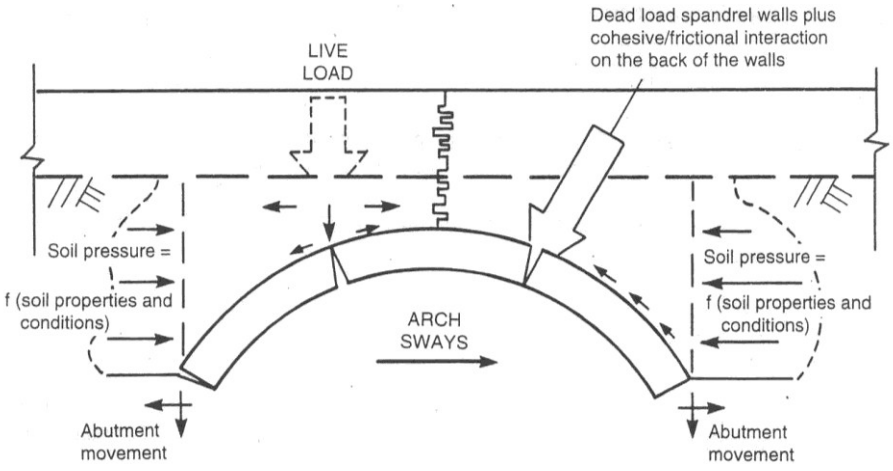

Figure 2- 2 Arch bridge response to dead and live load (Page 1993)

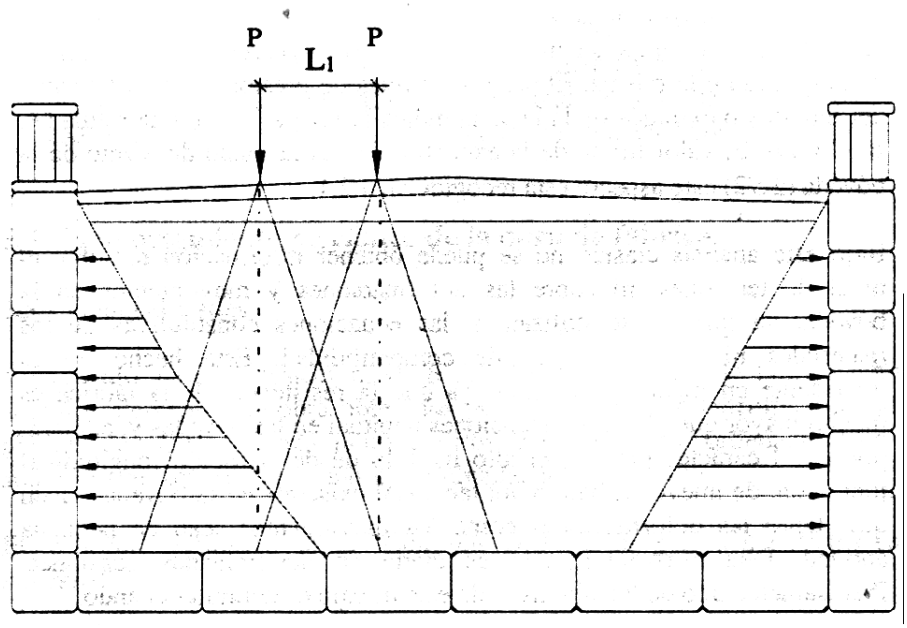

Figure 2- 3 Cross-section of a masonry arch bridge under load.

Figure 2-2 depicts the response of a masonry arch bridge to the dead load (self-weight) and a live load applied on ¼ of the arch's span. The dead load gravitated directly on the arch, whose shape approximates the curve of an antifunicular (this means that only compression is developed on the arch). The live load on the other hand, is transmitted from the road surface to the arch through the filling which cushions the effect of the load by transforming the load from a concentrated load to a spread load on the arch's extrados. Concentrated loads, and especially those in the critical zone (between 1/3 and 1/5 of the arch's span), tend to drive the geometry of the arch to adapt to the new configuration of actions (dead load plus the load), which causes the appearance of bending stresses, which in turn gives rise to thrusts that the masonry can not bear. The greater the amplitude of the cone distribution provided by the filling, the more decriminalized the effect of the concentrated load on the arch.

Another very important effect of the filling is the fact that it exercises an horizontal thrust on the spandrel walls, which in turn develop lateral pressures that are beneficial to the stability of the arch. This could cause failure of the spandrel walls by means of rupture of detachment from the arch. This would mean that the filling would no longer be confined and would not be able to develop its beneficial for the stability of the structure actions.

The spandrel walls except acting as retaining walls for the filling, also act like high stiffness beams. The interaction of these lateral elements with the arch can be very significant in situations close to collapse.

As mentioned before, once the load reaches the arch, the arch is responsible to transfer the loads to the foundation.

2.3 Analytical methods for the evaluation of masonry arch bridges

In this section, we will describe in brief the most commonly used methods of assessing masonry arch bridges. These methods have replaced the empirical experience of the past and have been devised to understand and predict the behavior of these bridges. The development of the assessment methods and theories derives from the evolution of understanding these structures.

Each method will be listed according to the theories and assumptions upon which they are based, elastic or plastic.

2.3.1 Elastic analytical methods

The elastic methods require the application of three types of equations to solve the structural problem: equilibrium equations, constitutive equations of the material (or materials), and equations of compatibility (in most cases difficult to establish if not impossible, because of ignorance of the actual boundary conditions of these bridges). The advantage that those methods have is the possibility to calculate the displacements and strains of the arch.

2.3.1.1 MEXE method

The MEXE method is mainly an extension of the theory of Pippard developed during the days of World War II. The Military Engineering Experimental Establishment (MEXE) method was first employed as a military load classification tool.

Pippard modeled the arch as linearly elastic with two pins at the abutments and applied a load at its mid-span (Ford et al 2003). Generally, the location of the critical load on an arch is at quarter-span. However, Pippard reasoned that load dispersion through the fill would shift the critical load to the location of the smallest fill depth, the mid-span (Page 1993). The hypothesis that the MEXE method considers are:

- The arch should have a parabolic guideline
- The arch is articulated on the abutments
- The ratio span/rise should be 4
- The arch bridge should be in a good condition

The MEXE method uses a nomograph based on the arch span and the crown thickness to derive a provisional axle loading, which is then modified by a series of parameters to yield a modified axle load. Some of these factors are highly subjective, such as the condition factor, a value which varies between 0 and 1 depending on the engineer's overall impression of the bridge state.

While the MEXE method is generally considered to be quick and over-conservative, the effectiveness of its semi-empirical approach is constrained by an inability to assess any but the most common bridge types.

2.3.1.2 Elastic frame analysis method

Unit width models of the arch ring provide quick, simple, and reasonably accurate strength assessments of a masonry arch bridge (Boothby 2001). Vital to this method are the material strength and stiffness constants that enable the predictions of bridge behavior. These values can be selected from recommended tables (Hendry 1990, Boothby 2001) or samples from the bridge site may be tested and evaluated. What MEXE lacks in adaptability to different bridge geometries is easy to overcome by the quick modeling interfaces in elastic frame analysis programs.

2.3.1.3 Elastic cracking analysis

The elastic cracking analysis is an analysis based on classical elastic theory in which the loads are applied in the arch and the stresses are determined. These are used to determine the state of stress, allowing the identification of stressed areas and areas where the material has been plasticized, which will allow then calculate the deformations and modified geometry of the structure. This allows modeling of snap-through failure, and pressure variations of the soil. The arch area, its inertia, the coordinates and applied load are updated later, and thus continues to iterate until converge. The effect of the soil is considered as a dead weight and as a constraint proportionally dependant on movement inwards or outwards of the infill, using the active and passive coefficients adapted to the geometry of the curve.

2.3.1.4 Finite element method

The finite element method has been the type of analysis that has recently been developed and extended in all variants of the structural calculations. Based on the Principle of Virtual Work (PTV) the displacements at the nodes are consistent with the boundary conditions imposed, and by interpolation, are found the displacements of the elements. With the PTV the equilibrium is found and then the stresses are calculated.

Besides the micromodels (that model of the mortar joints and the blocks separately), which are mostly useful in laboratory work, the most common is the use of macromodels,for which the masonry is considered as a unique material.

At first there were one-dimensional models with horizontal elements that took into account the filling. Later models with two-dimensional elements were used. These models are more suited to the study of the infill and are widely used today. Finally the three-dimensional models have a large computational cost and are only justified for very unique case studies. Their main problem is the difficulty of reproducing the concentrated deformation phenomena on certain points, as is the case of plastic hinges formed during the collapse mechanism of masonry

arch bridges. As a consequence, the equilibrium at advanced stages of loading can not be realistic, since it derives from the deformations of the elements.

2.3.2 Plasticity analysis methods

The plasticity analysis methods take into account the following assumptions:

i. The masonry has no tensile strength .Although the stone or the brick does have a tensile strength, in principle the masonry does not have, because the tensile forces can not be transmitted from one block to another through the joints.
ii. No slippage may occur between two blocks. In other words the line of thrust at each joint is almost orthogonal to it, so the tangential forces are not large enough to cause movement.
iii. The compressive strength of the masonry is infinite. This hypothesis goes against the security since the rock has a finite resistance to compression. However the error introduced is not very big since the stresses on the masonry arch generally not exceed 10% of the compressive strength, except locally in the areas of plastic hinges.

Under the assumptions the failure occurs when, a sufficient number of plastic hinges is formed and the structure is transformed into a mechanism.

2.3.2.1 Mechanism method

The mechanism method assumes that the bridge has infinitely rigid voussoirs and fails by the formation of hinges that turn the structure into a mechanism. The tensile strength of the masonry is assumed to be null and may include the passive earth pressure of the ground between the two hinges farthest from the position of the load.

This method is often used with computer programs with the load applied at one point and optimizing the positions of the four hinges so that the load is minimal. Changing the position of the load and repeating the process we can find the most unfavorable position for the structure and the critical load of collapse. This analysis is carried further by allowing the plastification of the hinges and taking the position of where the hinge spins towards the center of the plastic zone.

The results of this method are too conservative if not when you consider the collaboration of the infill. When one considers the collaboration of the infill, the results have a great variability depending on the coefficient of passive earth pressure which is adopted.

2.3.2.2 Limit state analysis

Masonry arch bridges are statically indeterminate compression structures which resist external applied loads primarily as a result of the thickness of the masonry and their inherent self weight. They tend to be resilient to small support movements, with these typically transforming a structure into a statically determinate form. Cracks which might accompany support movements are therefore not normally of great concern, making the notion of crack widths or other conventional serviceability criteria not applicable. Consequently engineers are generally primarily interested in guarding against the ultimate limit state (i.e. structural collapse) condition. This typically occurs when a sufficient number of hinges or sliding planes are present between blocks to create a collapse mechanism.

In masonry arch bridges which as noted before, are statically indeterminate structures there are infinite possibilities of equilibrium. The theorems used by limit analysis in order to find the equilibrium, are the upper bound theorem, the lower bound theorem and the uniqueness theorem. A sort definition of these theorems is given below.

Upper bound theorem: If a mechanism is assumed (by arbitrarily placing a sufficient number hinges), the load which results from equating the work of the external forces to zero is an upper-bound of the actual ultimate load

Uniqueness theorem: The collapsing configuration will be reached if a thrust line can be found causing as many plastic hinges as needed to develop a mechanism. Plastic hinges are caused by the thrust line becoming tangent to the boundaries. When this occurs, the load is the true ultimate load, the mechanism is the true ultimate mechanism, and the thrust line is the only possible one

Lower bound theorem: The structure is safe, meaning that the collapse will not occur, if a statically admissible state of equilibrium can be found. This occurs when a thrust line can be determined, in equilibrium with the external loads, which falls within the boundaries of the structure. The load applied is a lower bound of the actual ultimate load (causing failure).

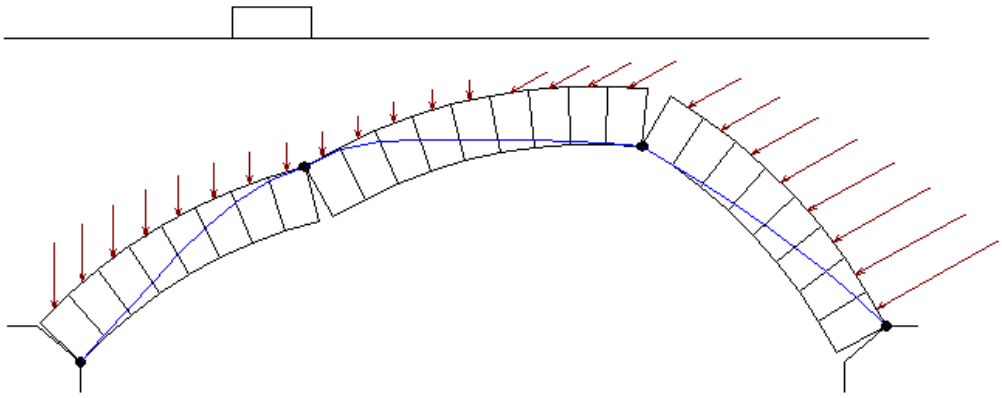

Figure 2- 4 Four hinge mechanism and thrust line of a one span masonry bridge (Ring 1.5)

The limit analysis basis is on finding a thrust line inside the arch. Under such conditions the Lower bound theorem allows us to state that the structure is stable. When the thrust line becomes tangent to the arch on four point (assuming that the analyzed arch is fixed-ended) the Uniqueness Theorem assures us that the line of thrust found is unique, and therefore is real one.

This type of analysis is very powerful because it allows to obtain the collapse load and the location of the plastic hinges to form the collapse mechanism, only through the application static equations (equilibrium equations).

We have to note that the limit analysis program RING which was used for this thesis, uses the concept described before.

3. EXPERIMENTAL PROCEDURE AND RESULTS

3.1 Introduction

In this chapter, we will describe the work performed in the Structural Technology Laboratory of UPC in the course of the experimental preparation and execution of the masonry arch bridge subject matter of this dissertation.

The first section discusses in detail the dimensioning of the bridge, the materials used in its construction and the construction process itself. This will need to rely on photographic material and documentation from the previous specialty dissertation framed in the same season of experimentation, “Experimental Analysis of the bearing capacity of a masonry arch bridge” (Alexandre Rodriquez Castiblanque).

The second part describes the instrumentation used during the test; explains what are the parameters measured with each instrument and the reason for which it was used. The same section describes the method of load application.

Finally, all the data obtained from the experimental procedure are presented and discussed. Moreover a limit analysis of the masonry arch bridge is presented.

3.2 Construction procedure of the masonry arch bridge

The bridge which consists the matter subject of this dissertation was the second to be studied within the experimental campaign of masonry arch bridges led by Professor Pere Roca, Department of Construction Engineering of UPC.

The bridge was designed in 2002 and its construction (which involved staff of the Laboratory of Structural Technology) was performed during the academic year 2002 -2003. Its testing until collapse was held on Thursday July 10, 2003.

3.2.1 Geometrical description of the bridge

The dimensioning of the bridge was made taking into account the constraints of space, availability and capacity of the test apparatus, especially the loading gantry, and, of course, the budget control which is very high in this type of tests. The characteristics of this half-point bridge, were similar to those tested before, trying to approximate the characteristics of the arch bridges studied by Ernest Soms, in order to be able to compare the theoretical results with those obtained experimentally during the test. That was precisely one of the main objectives of the testing program on masonry arch bridges developed in the Structural Technology Laboratory of UPC.

The main dimensions of the bridge are listed below:

- Total length of bridge: 5.2m. This dimension includes the length of the ears which extend 1m each side from the end of the intrados of the arch.
- Free span of the arch: 3.2m.
- Rise in the center of the arch span: 1.6m.
- Thickness of the arch ring: 0.14m. The thickness is constant throughout the range and equal to the width of the brick.
- Thickness of the filling above the key 0.1m.
- Thickness of the filling above the abutments: 1.85m. This thickness refers to the total height of the filling of the arch above the abutments. It consists of a cementitious filling of 0.68 meters tall and, above it, compacted sand filling of 1.17 meters.
- Total height of the bridge: 2.15m. This dimension includes the height of the foundation slabs in which abuts the arch. The foundation slabs are concrete slabs of 1m quadrangular plan, with 0.17m high in the first step and approximately 0.18m height in the second step.
- Thickness of the spandrel walls: 0.14m. Again, this dimension coincides with the width of the bricks which were used to build the bridge.
- Filling width (distance between the inside surfaces of the spandrel walls): 0.72m.
- Total bridge width: 1m.

In figures 3-1 and 3-2 the sketch of the semicircular bridge and the foundation slab can be observed.

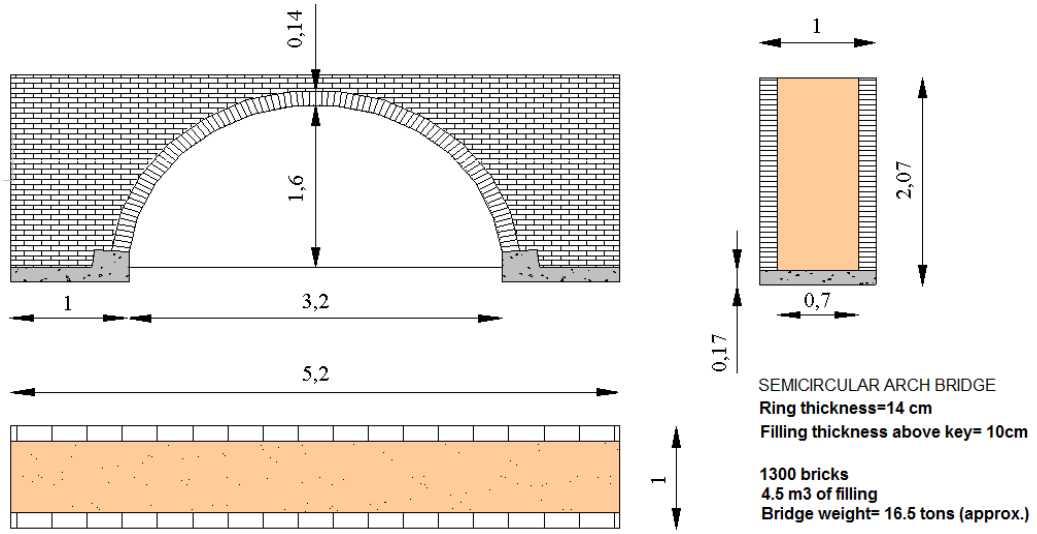

Figure 3-1 Geometry of the semicircular bridge tested in the Structural Technology Laboratory of UPC (dimensions in meters).

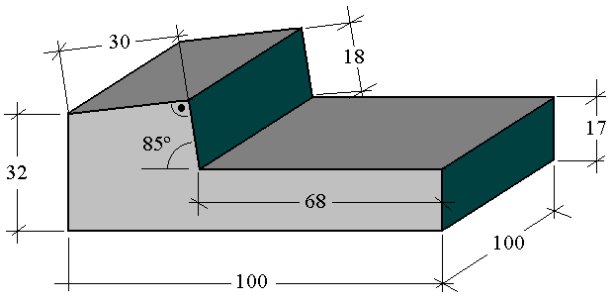

Figure 3-2 Geometry and dimensions of the foundation slab of the bridge (dimensions in cm.).

As shown in the figure 3-1, it is a semicircular arch, with an accurate ratio of span / rise equal to ½. The spandrel walls extended 1m beyond the arch intrados to properly simulate the action of filling in the abutments.

The slabs were designed as a ladder with two rungs and with a certain inclination on the highest step, so that the surface was perpendicular to the arch at that point and thus perfectly fit the thread between the two slabs. In this way was achieved the lower level of the abutment to work as a foundation slab and the upper to materialize a transition point.

Two profiles were used at the lower part of the foundation slabs that worked as constraints set against rotation. In addition to these profiles, we used two metal structures to ensure the containment of the two types of filling during construction, and to confine them during the test implementation.

A summary of the geometrical and construction features of the bridge are shown in the following table.

Geometrical feature	Value
Free span (m)	3.20
Rise (m)	1.60
Total length (with abutments) (m)	5.20
Total height (m)	2.15
Width (m)	1.00
Ring depth (m)	0.14
Depth of infill on crown (m)	0.10
Depth of backings on abutments (m)	0.81
Maximum depth of un-cohesive infill (m)	1.17
Thickness of spandrel walls (m)	0.14
Number of steel ties (φ=25mm)	8
Loaded point	¼ of span

Table 3-1 Summary of the geometrical and construction features of the bridge

3.2.2 Materials used for the construction of the bridge

In this section the list of materials used to construct the bridge in the laboratory is presented:

- The bricks used to construct the spandrel walls as well as the ring of the bridge were solid bricks of 13.5cm x 28.5cm x 4.5cm thick and Catalan-like type. Approximately about 500 bricks were used to construct all the elements of the bridge. The structure configuration used for the arch ring is shown in Figure 3-3. The compression and shear resistance of these structures, which were studied in the Structural Technology Laboratory of UPC, were 19.6MPa and 0.363MPa correspondingly.

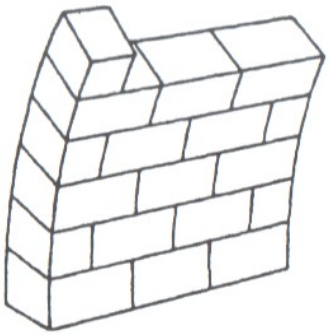

Figure 3-3 Structure configuration used for the arch ring

- The mortar used for the joints between the bricks of the structure was an M-8 Portland cement mortar. The bed joints were 1-1.5cm thick.
- To build the foundation slab, which supports the arch and the spandrel walls about 450 liters of concrete were used. These slabs were armed with bars of B 500 S, with a total weight of steel of approximately 40kg.
- The loose backfill was materialized with a sand of loose type which is in common use in the production of concrete. Its dry density was of 1560kg/m^3 and its Proctor density, that is the one that tried to obtain by means of the compaction of the backfill, was of approximately 1880kg/m^3. The total volume of necessary sand to fill the bridge among it spandrel walls and the arch and the cemented backfill was of approximately 3m^3.
- The mortar used to manufacture the backfill over the abutments was an M-8 mortar with average diameter of granular material was approximately 20mm. The total volume of mortar used for the implementation of the backfill was approximately 1.5m^3.
- Steel plates stiffened with steel profiles were installed at the back sides of the abutments to retain the infill . A set of ties, consisting of steel bars with diameter of 25 mm, where anchored to the horizontal profiles stiffening the plates. These ties are used to simulate a possible external lateral confinement at the ends of the bridge caused by possible masonry walls extending beyond the abutments or the natural soil.

Table 3-2 shows values measured on different material properties obtained by tests carried out on elementary mortar, brick and masonry specimens. In particular, the properties of the mortar-unit interface have been more recently determined by testing couplets with biaxial testing equipment.

Component	Property	Average (N/mm^2)	Type of specimen
Brick (longwise) Brick (flatwise)	Compression strength Young modulus Compression strength Young modulus	56.8 12,750 51.0 10,450	40x40x120 mm prisms 3 stacked 40 mm cubes
Mortar	Compression strength Flexural strength Young modulus	8.34 2.68 810	Prismatic 40×40×80 mm Prismatic 40×40×160 mm
Joint interface	Cohesion Cohesion Initial friction angle Residual friction angle	0.36 0.33 45º 37.2º	triplet couplet (biaxial equipment) “ “
Masonry	Compression strength	14.0	4 flat brick prism
Infill (sand)	Specific weight	18 kN/m^3	

Table 3-2 Information on material properties and testing procedures

The total number of elements used and their dimensions are as follows.

1. Retaining structures of the compacted granular backfill:

- 2 metal sheets with dimensions of 100 x $100cm^2$ and 5mm. thick.
- 10 vertical profiles. These profiles are tubular and hollow with side of 5 cm, 4mm thickness and 100cm length, and were bind to the plate before welding.
- 8 horizontal profiles welded to the vertical. These profiles are tubular and hollow with horizontal sides of 140 x 80mm, 6mm thick and 118cm. long. All were drilled at the ends for threading the bars which should join the metal plates on either sides of the bridge.
- 6 bars with diameter of 25mm, 580cm long mechanized in their extremes, to thread the horizontal tubular profiles and the corresponding 12 nuts (2 for each bar).

2. The filling retaining structures:

- 2 metal sheets with dimensions of 100 x $100cm^2$ and 5mm. thick.
- 8 vertical profiles. These profiles are tubular and hollow with side of 5 cm, 4mm thickness and 100cm length, and were bind to the plate before welding.
- 2 horizontal profiles welded to the vertical. These profiles are tubular and hollow with horizontal sides of 140 x 80mm, 6mm. thick and 118cm. long. All were drilled at each ends for threading the bars which should join the metal plates on either sides of the bridge.

- 2 bars φ25, 580cm. long mechanized in their extremes, to thread the tubular profiles and the corresponding 4 horizontal nuts (2 for each bar).
- Two profiles UPN 220 of 5.2m length for the bracing of the foundations against rotation. To attach these two profiles to the slabs 4 bars with diameter of 30mm were used, and were arranged inside of them during their construction, and the corresponding threads.

The approximate weight of the bridge, having used the materials and quantities of materials listed before, was estimated at 17 tones.

3.2.3 Bridge construction process in the laboratory

The first element to be constructed was the reinforced concrete slabs on which the starters would be supported on and that had to collect the reactions that the arch would transmit. The reinforcement consisted of bars with diameter of 20mm of 20cm length each, to resist the bending; 16-pins with diameter of 10mm with equal distribution area in each of the two slabs to withstand the shear and, for the control of the retraction a minimum reinforcement in the form of bars with diameter of 8mm was arranged. In addition to this mesh, two threaded crossbars of 20mm were arranged in each footing (Figure 3-3). These bars were part of the bracing system of the bridge, which will be explained in more detail in Section 3.2.4.

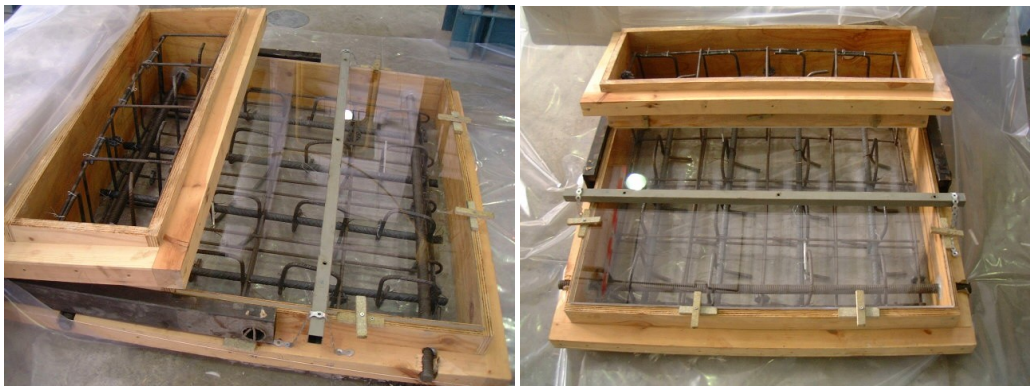

Figure 3-4 Mesh and formwork of the concrete slabs.

The slabs were constructed with high-strength concrete (80Mpa) with superplasticizers to facilitate their installation and shaping. The total volume of concrete required was approximately 450 liters. The fluidity of the concrete and adjustment to the geometry of the slabs are shown in the figure.

Figure 3-5 Construction of the concrete slabs

These slabs, as already mentioned, played the role of foundations and abutments at the same time. Its ground plan was $1m^2$ with a thickness of 17cm at the first step (which served as foundation) and 18cm at the second one (the one acting as abutment). On this second step, of surface of 30 x $18cm^2$ and with an inclination of 3^o with respect to the horizontal, rested the first voussoir of the arch. This inclination was necessary to ensure proper connection between the abutment and the arch, and thus to make possible the embedment of the arch (Figure 3-6).This embedment ended with the bracing system.

Figure 3-6 Detail of the starting of the arch on the foundation slab.

Once the concrete was hardened and a minimal resistance was acquired, we moved to the construction of the brick elements of the arch and spandrel walls. In Figure 3-7 you can see the dimensions of the wood framing selected for the construction of the vault and a picture of it.

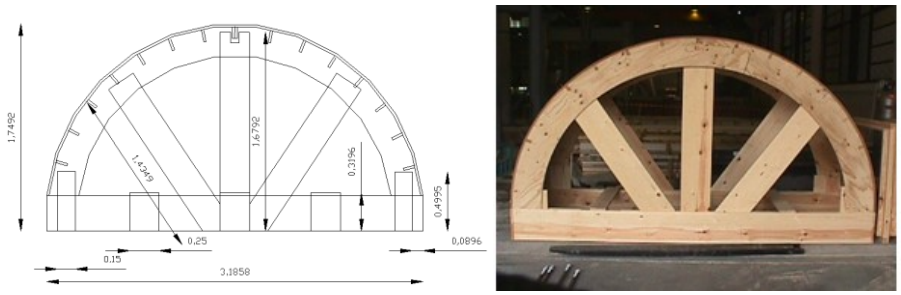

Figure 3-7 Sketch of the formwork for the vault. Image of the formwork once finished.

After removing the formwork of the concrete slabs, the formwork of the arch was positioned between the slabs and then starts the procedure of the placement of the bricks that form the arch ring. In Figure 3-8 you can see the finished ring. After the ring, we proceed to the construction of the spandrel walls. The same figure shows the construction of spandrel walls.

Figure 3-8 Finished ring and construction of the spandrel walls

In Figure 3-9 you can see the concrete slabs and the masonry structures finished. All the work to this point was made by German de Marco and laboratory personnel.

Figure 3-9 Finished brickwork of the semicircular bridge.

Once the construction of the reinforced concrete slabs and the brickwork was over, the next thing to be done, was the procedure of the removal of the formwork (formwork of the arch). This operation should take place before of the placement of the filling, as its weight, together with the efforts that could be developed during the actual placement and compaction could lead to minor deformations of the formwork so that it could not be removed later.

To remove the formwork one of the profiles constituting the bracing system was positioned. This was done due to ignorance of how the operation of decentering would affect the state of the bridge. In fact, it could be the case that the efforts made on the formwork would be transmitted to the brick causing the loading of the arch came into effect which in turn would be partially restrained by the metal bracing system, responsible in this time of providing lateral resistance to the whole. The removal of the formwork was achieved by pulling from both ends at the same time, thus reducing the maximum contact between the formwork and the arch

during the operation. The delicacy of this action made the total decentering operation of the structure last about an hour and a half. In Figure 3-10 different stages of the operation of decentering can be observed.

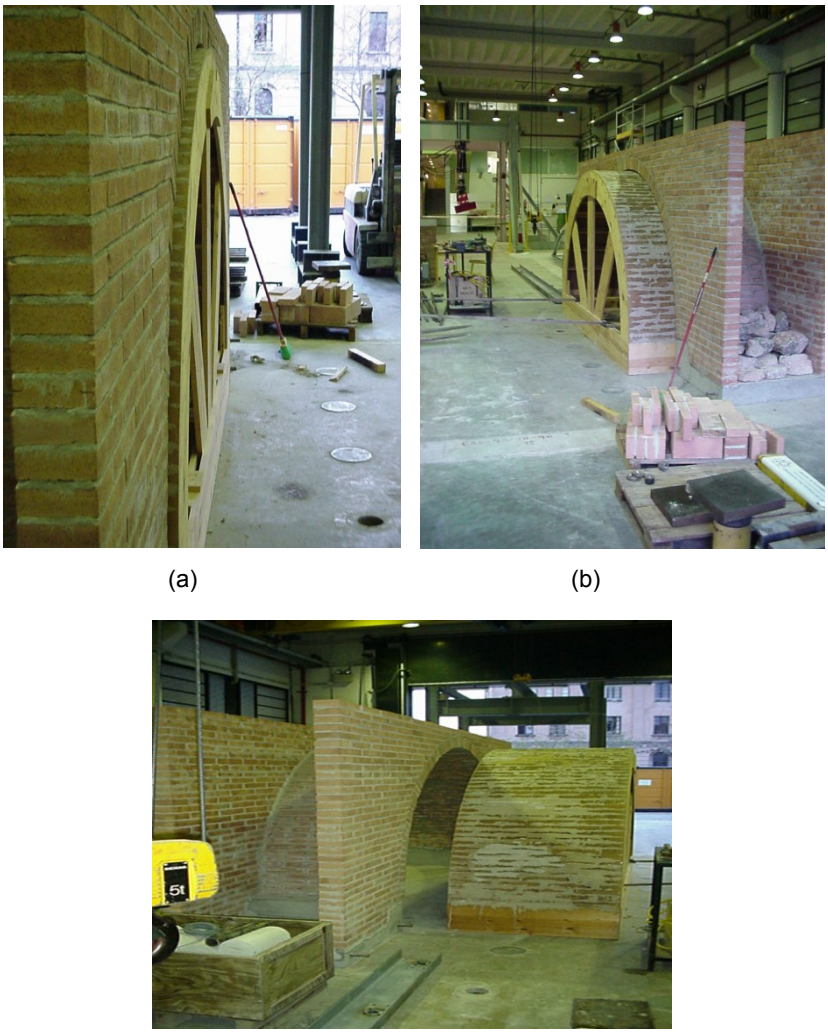

(a) (b)

(c)

Figure 3-10 Decentering of the arch of the bridge. (a) Result of manual decentering after one hour, (b) Result of decentering using a torus after about 1h15', (c) total arch decentering after 1h30'.

In order to use the UPN bracing profiles, they had to be adapted by drilling in the appropriate locations, so that they could be attached to the bars arranged in the foundation slab for this purpose. Once the bridge decentering was over, both profiles were placed (the entire bracing structure) in order to continue working on the preparation of the bridge, so that if efforts on it were exerted would be absorbed by the two profiles.

Figure 3-11 Detail of the drilling of the UPN profiles. In the background you can see the bars included in the foundation slab for the placement of the bracing profiles.

Once arrived at this point we were ready to place the metal sheet structure in the abutments. These structures were sized during the first trial of a segmental bridge (Figure 3-12), conducted by José Serna and Hector Gutierrez. Initially the stiffened metal sheet structures by means of hollow structural steel sections were intended for two purposes. The first was to contain the filling during its positioning, and the second was to, resist the thrust exercised by the filling as a result of applying the load. It was this second condition which governed their design (during designing, it was considered that the filling could get to fully develop the passive earth pressure). However, the metal structure did not work as expected. Indeed it was more than able to withstand the thrust developed by the filling, but did not prevent the rotation of the slabs during the test implementation, converting the arch which had originally been considered as fixed-ended in an arch bi-articulated.

For that reason in the second experiment of the segmental bridge, after repair and refurbishment, German de Marco sized a new bracing system to prevent the movement of the foundation slab in the starters of the arch. The bracing system composed of the UPN will be explained in detail later. Thus, metal sheet structures reduced their role to hold the filling during positioning and resist the thrust of it during the application of the load. Moreover, the filling containment structures were sized for the most unfavorable situation for both bridges.

Figure 3-12 Elements and manufacture of the metal sheet structure, for the containment of the filling during the preparation of the first test of the segmental bridge.

The only drawback of stiffened plates was the need to be duplicated because of the bridge's greater height respect to the segmental one. A new structure, which was lighter and less stiffened than necessary in the upper part of the bridge, was created.

In the first place the plates on the ends of the abutments were settled for the containment concrete. These two plates were joined only by two bars φ25, 580cm long, with their extreme ends machined in order to screw them. The system worked as it was designed to work, and it contained the concrete during positioning and curing it.

During the curing of the concrete we proceeded the placement of the portal of load in its position. This operation had to be done carefully to avoid damaging the skinny walls during the movements of the great mass of steel which represents the loading frame.

Once the concrete had sufficient strength we passed to the assembly of the metal structure which would contain the granular fill.

The granular filling used was composed of a sand type, which is commonly used in the production of concrete. These sands were characterized to some extent in order to decide on the form of compaction. Its dry density was 1.56t / m^3. To obtain the optimum moisture of the filling a Standard Proctor was performed in the Laboratory of Transportations of UPC, in accordance with the NLT-107/91 regulatory. The results obtained showed an optimal humidity of approximately 6% and a maximum Proctor density of 1.88t / m^3.

The results obtained in the test and the Proctor curve density-moisture are shown Table 3-3.

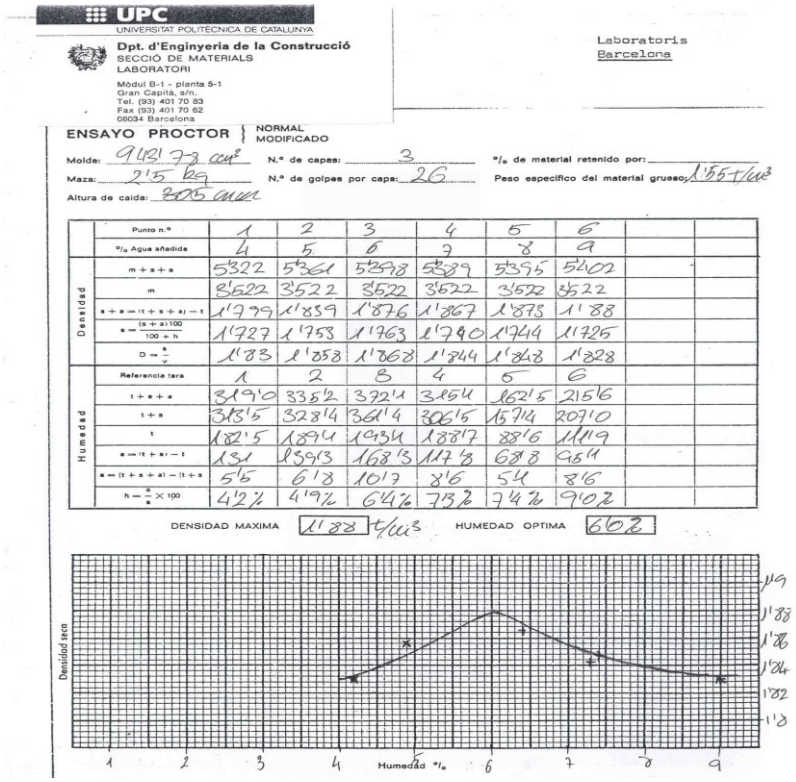
UPC
UNIVERSITAT POLITÈCNICA DE CATALUNYA
Dpt. d'Enginyeria de la Construcció
SECCIÓ DE MATERIALS
LABORATORI
Mòdul B-1 - planta 5-1
Gran Capità, s/n.
Tel. (93) 401 70 83
Fax (93) 401 70 62
08034 Barcelona
Laboratoris
Barcelona
ENSAYO PROCTOR } NORMAL MODIFICADO
Molde: 9483 73 cm³ N.º de capas: 3 °/₀ de material retenido por:
Maza: 2'5 kg N.º de golpes por capa: 26 Peso específico del material grueso: 1'55 t/m³
Altura de caída: 305 mm

	Punto n.º	1	2	3	4	5	6
	°/₀ Agua añadida	4	5	6	7	8	9
Densidad	m + s + a	5322	5361	5398	5389	5395	5402
	m	3522	3522	3522	3522	3522	3522
	s + a = (t + s + a) − t	1'799	1'859	1'876	1'867	1'873	1'88
	s = (s + a)·100 / (100 + h)	1'727	1'753	1'763	1'740	1'744	1'726
	d = s/v	1'83	1'858	1'868	1'844	1'848	1'828
Humedad	Referencia tara	1	2	3	4	5	6
	t + s + a	319'0	335'2	372'1	325'4	162'5	215'6
	t + s	313'5	328'4	361'4	306'5	157'4	207'0
	t	182'5	189'4	193'4	188'7	88'6	111'9
	s = (t + s) − t	131	139'3	168'3	117'8	68'8	95'1
	a = (t + s + a) − (t + s)	5'5	6'8	10'7	8'6	5'4	8'6
	h = a/s × 100	4'2%	4'9%	6'4%	7'3%	7'8%	9'0%

DENSIDAD MAXIMA 1'88 t/m³ HUMEDAD OPTIMA 6'0%

Table 3-3 Standard Proctor test results conducted on the granular filling material. Density-moisture curve obtained.

Once assembled the necessary structure and with the Proctor data known the placement and compaction of the filling inside the bridge could be started. The process used to introduce the filling was the following:

- The compactor which was used in this test was of greater power than had been previously used in other tests on masonry bridges in UPC. This enabled the compaction of the fill in layers of greater thickness. In this case it was decided to pour the loose material inside the bridge and to compact in layers of 20cm.

- The volume of compacted sand needed to form each one layer of 20cm had been calculated previously. The volume of compacted sand was transformed to the volume of loose sand. By knowing the optimum moisture and the maximum Proctor density, which was to be reached, one could calculate the necessary volume of water in each layer in order to achieve the desired compaction. The mixture was made in the interior of the bridge. Firstly, the necessary amount of sand was poured, and then the volume of water needed was added, with the help of a flowmeter placed in a hose. The mixture was knead to try to make it as homogeneous as possible. In Figure 3-13 you can see the hose attached to the flowmeter to control the volume of water introduced for each layer.

Figure 3-13 Flowmeter used to control the moisture.

- Once the mixture was considered to be homogeneous we proceeded to its compaction. The device used to compact the filling, had to be rent because it was not available in the laboratory. This apparatus provided the necessary energy for the compaction by means of impact and vibration. Given the great energy that was to be provided it was decided to manually compact the zones of filling in areas close to the masonry (arch and spandrel walls). For the manual compaction of the filling one of the rams available in the laboratory was used.

Figure 3-14 Sixth layer of compaction. On the left you can see the sand before achieving the homogenization of the layer. On the right you can see the layer already homogenized and compacted.

The final result was the use of approximately $3m^3$ of sand and about 180 liters of water spread over 5 layers of about 20cm each.

In tests earlier this campaign measures of the densities achieved in the different layers had been taken from an approximate method. Knowing the density and humidity of each layer allows us to obtain the CBR of the soil and, from this, to get an approximation of the modulus of elasticity of the filling. In this test the aim was to compare the ultimate capacity of the bridge with that obtained from numerical models, so it was not necessary to fully characterize the filling.

3.2.4 Bridge bracing system

During the previous experimental campaign on a segmental arch bridge, conducted by José Serna and Hector Gutierrez, appeared certain problems that hampered much the discussion of the results. Since the early stages of loading a slight lifting of the concrete slab in the area farthest from the starting point of load application was noticeable. When reached load of 6t the lifting of the slab became clear. But it was when he arrived at 7 tons of cargo that they were aware of the problem when sudden lifting of the two concrete slabs occurred. The interpretation of what occurred could not be other than the fact that the bridge, which was considered as fixed-ended in order to calculate the ultimate capacity, it had become a bi-articulated bridge due to the possibility of rotation of its foundations (Figure 3-15).

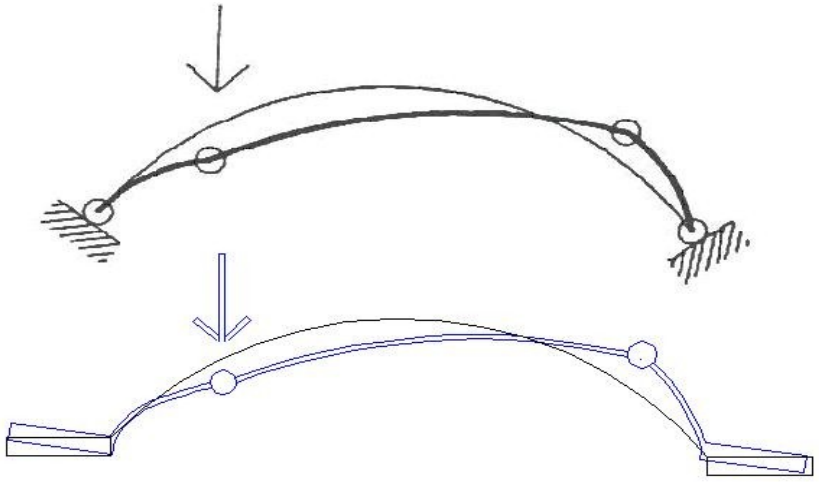

Figure 3-15 Expected failure mechanism in the Gutiérrez-Serna bridge. Actual mechanism with the formation of only two plastic hinges.

Once the bridge was bi-articulated only the formation of two plastic hinges was necessary to complete the collapse mechanism. This fact is supposed to reduce the ultimate capacity of the bridge.

Given these facts, a bracing system that could prevent the rotation of the bridge's foundations was designed. This system consisted of a pair of metal beams, one on each side of the bridge connected to it through the concrete slabs.

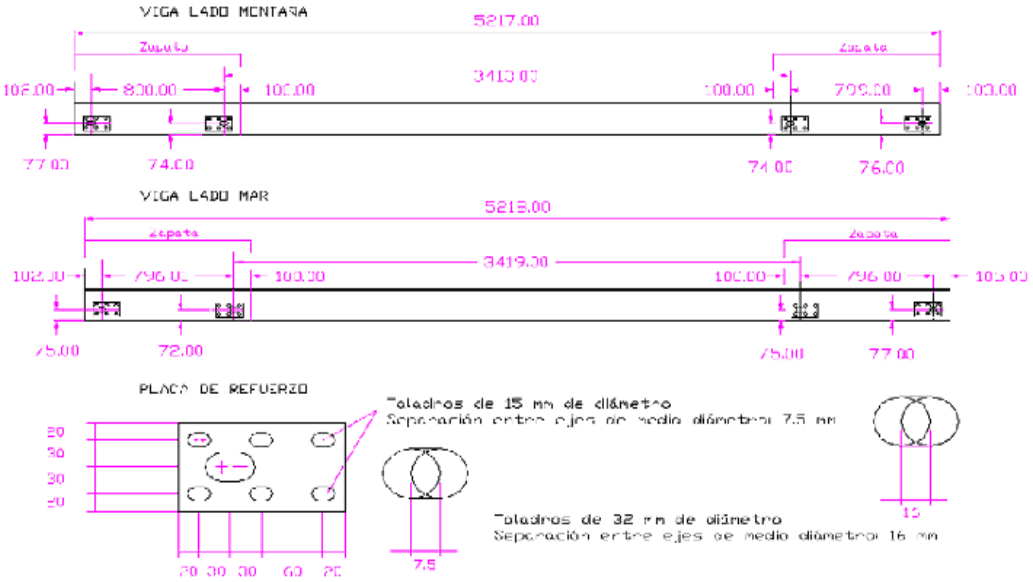

Figure 3-16 Sketch of the UPN dimensions by German de Marco.

The relevant calculations for the sizing of the beams were performed for a load of 12 tons and the worst load case (load that far exceeds the expected ultimate load for both bridges).

The final result was two profiles UPN 220 of steel A-42 that, that in the case of the semicircular bridge, were connected to the concrete slabs by means of bars with diameter of

30mm already arranged in the slabs during their construction. The bars were verified also, in their connection with the profiles, against cutting, crushing and tearing.

Figure 3-17 Positioning and testing of the bracing system before decentering.

3.3 Instrumentation of the semicircular arch bridge

Compared to other studies so far the degree of instrumentation was low. The instrumentation and monitoring of the behavior of the bridge of course depend on the availability of measuring instruments in the laboratory at the time of experiment. But nevertheless, the most compelling reason for not having a very complex instrumentation was that the best interest of the test focused on determining the collapse load and observing the failure mechanism in order to compare observations with results of the program of numerical calculations designed by Ernest Soms. In this sense, the instrumentation of the trial was sufficient.

The instrumentation used to record the test results was as follows:

- A cylindrical load cell under the hydraulic jack to measure the applied load.
- Three extensometers to measure the displacements in different points of the bridge during the process of the load implementation. One was positioned under the point of load application, one in the center arch rise and the third in the point symmetrical to the point of load application with respect to the central arch rise.
- A transducer of relative pressure, that for more security provided a second value of the load cell. In fact, this equipment recorded values slightly different from those taken by the load cell, because this equipment was connected directly to the jack so that the hydraulic pressure measured was the latter received.

In addition to this equipment an information processing equipment was used to store and display readings recorded by the instrumentation. We also used another information processing equipment to view and control the load that was applied by the hydraulic unit.

Despite the fact that it would have been interesting to analyze results, no load cells were used to measure the tension undertaken by the bars of the filling containment system, because it was considered that most of the horizontal thrust would be absorbed by the bracing profiles.

3.3.1 Gauges for measuring displacements

Three strain gauges were used to measure the vertical displacements in three points of the arch bridge, since the moment that the process of applying the load started. They were located in the two points likely to suffer larger displacements and under the key, which is always located on half the span of the arch.

The transducers placed under the load and the point symmetrical to it with respect to the central rise had the capacity to measure 100mm vertically upwards and downwards respectively. These two gauges were the most capable, since these two points are, in principle, which must undergo larger displacements. The third one was placed under the key of the arch. This extensometer was equipped with the ability to measure upward but did not have the capability for such large measurements as the ones discussed before, because it was believed that the movements recorded on the key would be lower.

The intention during the test was to remove the strain gauges just after the fourth plastic hinge of the collapse mechanism was formed. However, the formation of the mechanism damaged the bridge to such an extent that it was decided at the danger of total collapse of the structure, not to risk removing the extensometers and move to the second phase of the trial. The result was the loss of the three strain gauges.

Figure 3-18 Extensometers placed under the arch. Detail of the main core of the strain gauges. Detailed contact between the bridge and the transducer.

3.3.2 System for the application and the measurement of the load

To apply the load to a distance of ¼ of the arch's span a hydraulic jack was used, with capacity for a point load of 60 tons.

The reaction of the jack was supported by the load portal which in turn transmitted it to the laboratory load slab load by 16 pretensioned. The system for the application of the load is shown in Figure 3 -19.

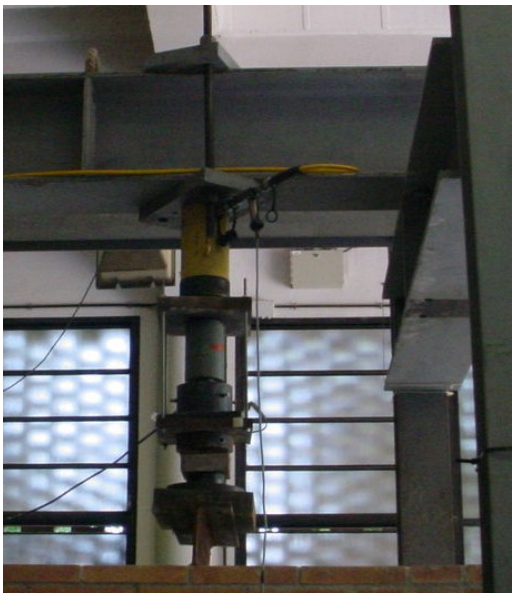

Figure 3-19 System for the application of the load

Under the jack is placed between two plates, a load cell in order to monitor the application of the load. Below there is a steel plate of rectangular shape of about 8cm thick. Under this plate a system consisting of a spherical hinge attached to another plate was arranged. The spherical hinge ensured that the load would be symmetrically transmitted.

Under the hinge (the mechanism formed by the hinge and the last plate) the last profile was arranged. This profile was a HEB 200 placed horizontally and trimmed in such a way that it would transmit the load in the form of a knife across the width of the bridge without actually affecting the spandrel walls directly (since they would be affected as the load is spread in depth through the filling).

3.3.3 Data processors

In total we used two computers, one for data acquisition and monitoring and one for the load control of the jack. The reading of the data obtained from the load cell and strain gauges reached the PC through a data acquisition card. Also two different power supplies were used.

Finally, the displacements of the three gauges were monitored on a computer, while the applied load was monitored on two PCs and other electronic recording devices.

Upon completion of the entire installation, and before the beginning of the test, tests were performed to verify the correct operation of the instrumentation and data acquisition system. Also calibration of all the instruments had to be performed.

Figure 3-20 Processors and data acquisition equipment. Relative pressure transducer. Hydraulic pressure supply.

3.4 Execution of the test

On July 10, 2003 the bridge was ready to be tested by loading it until collapse. The loading process is recorded on video. The intention was also to take pictures showing the development of the cracks during the test performance, but due to technical problems, it was not possible. The photographic record shows only images of the state of the bridge after the first and second load cycles.

Figure 3-21 Aspect of the bridge, moments before the start of the test.

3.4.1 Load application process

3.4.1.1 First cycle of loading

The load began to be applied at a rate of 0.05bares / second, which, given that the surface of application of the load together with the jack was 82cm^2 is equivalent to a loading rate of about 0.25tones / min (about one tone every four minutes).

Due to some technical fault the loading system did not work as expected. It remained relaxed for about 20 minutes to increase the load up to 4 tons in seconds, recording a peak speed of loading of 40tones / minute. Given the speed of the events the test stopped. When the hydraulic pressure stopped, the load on the bridge exerted 9 tons and had already formed the collapse mechanism.

The final result was the subsequent formation of cracks and the four plastic hinges that should form the mechanism could not be recorded in time. This is the reason why a relationship between levels of damage and loading can not be established. However, it is possible that the ultimate load of 9.2tones recorded is correct. The speed with which the charging process occurred was also the reason why it was impossible take successive pictures of the cracks and the order of formation of the plastic hinges.

Although the ultimate load was about 3 times the expected one, the final collapse mechanism itself was the one expected. Although, it is not known the exact sequence of formation of the plastic hinges, it can be said that they developed in areas expected.

Figure 3-22 shows some of the cracks and the hinges formed during the first circle of loading.

Figure 3-22 Views of the separation of the arch ring. A greater separation under the point of loading is obvious. Longitudinal cracks of the spandrel walls. Plastic hinge under the load and opposite to it.

3.4.1.2 Second loading cycle

The second charge cycle began once enough time had passed for the structure to relax and recover the elastic deformations suffered. It was decided to reapply a loading rate of 0.25tones / minute.

The interest of this second loading cycle was focused on knowing how much load the semicircular bridge could withstand once the collapse mechanism of four hinges was fully formed. Knowing the damage suffered by the bridge during the first loading cycle, it was assumed that no new cracks would be formed and, of course, no more hinges would be formed.

Indeed, during the second loading cycle no significant change in the geometry that the bridge had acquired during the first loading cycle was observed. There were only observed small amplifications of already existing cracks. The total collapse of the structure came for a load close to 1.4tones, or approximately 15% of the load required for the formation of the collapse mechanism in the first loading cycle.

3.5 Analysis of the test results

3.5.1 Data on the applied load

The first loading cycle began, in theory, with a constant load rate of 0.25tones / minute, but because of a technical problem the load started suddenly to increase linearly in time. This can be seen in Figure 3-23, which shows the graphs obtained from recorded data by the load cell.

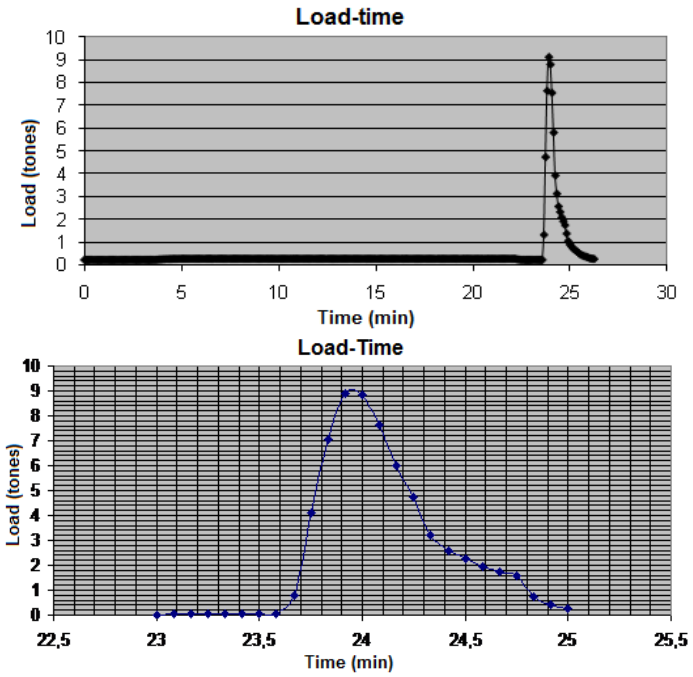

Figure 3-23 Evolution of the load over time (Figure obtained from the load cell). Detail of the process of load increase in the phase of rapid advance.

It should be noted that once the test stopped, the load dropped sharply. The downloading speed is much slower than the loading procedure and consequently increases the time that the bridge must support an action of considerable magnitude. In fact, according to preliminary calculations, the structure had to withstand up to 3.25 tons, a value that was exceeded for at least half a minute.

During the second loading cycle, it was decided to apply the load with a rate of 0.25 tones / minute However, as shown in the graph of Figure 3-24, pressure was applied on the structure almost immediately after giving the order to the hydraulic jack and for the second time the load is not exercised at a constant speed as indicated by the computer system governing the hydraulic unit.

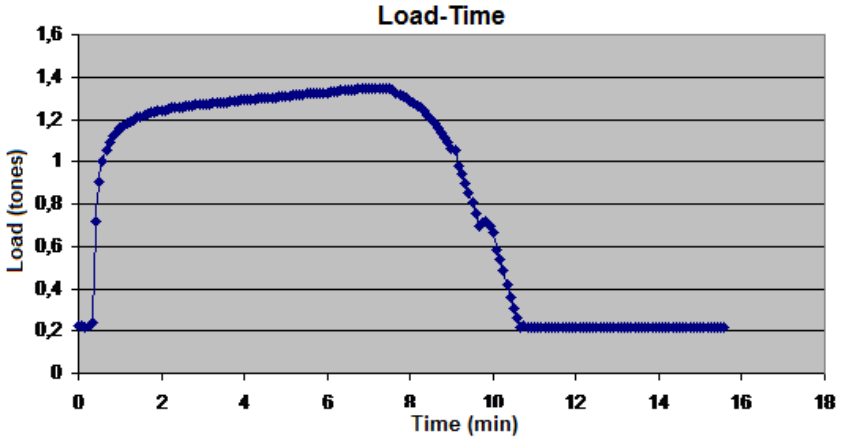

Figure 3-24 Graphs of the second charge cycle. Recorded data of the load cell

Only about 1.4 tons was reached in the second loading cycle. This indicates that the bridge had reached the collapse state since the first loading cycle that the mechanism of four plastic hinges was formed.

3.5.2 Data on the displacements of the arch

In the following figures are shown the data recorded by the three strain gauges during the first loading cycle. The strain gauges were placed in the central longitudinal axis of the arch at distances of ¼, ½ and ¾ of the span of the bridge and measured the vertical displacements. During the loading of a masonry arch bridge there are also horizontal movements, which in any case, are smaller and less interesting.

It is worth mentioning that not all the data recorded during the first cycle were incorporated in order to avoid a great deal of data. Only records taken since the moment that the bridge comes under load have been plotted.

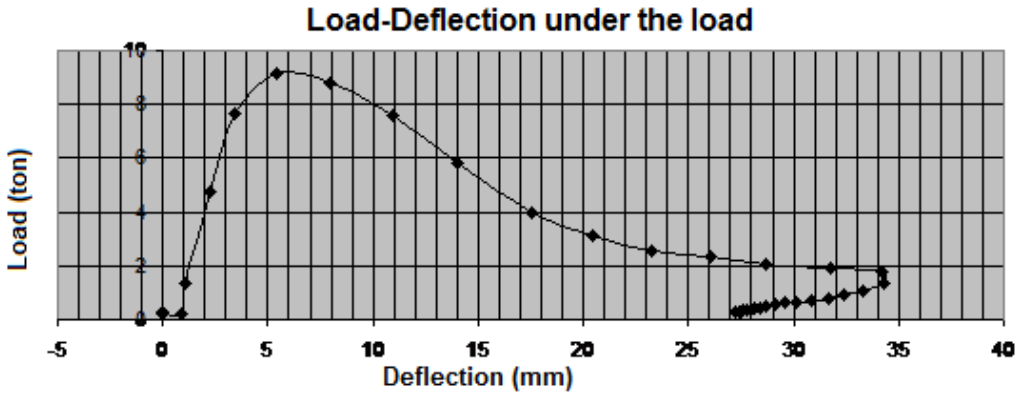

Figure 3-25 Relation load-deflection under the point of load application. Positive deflection indicates decline.

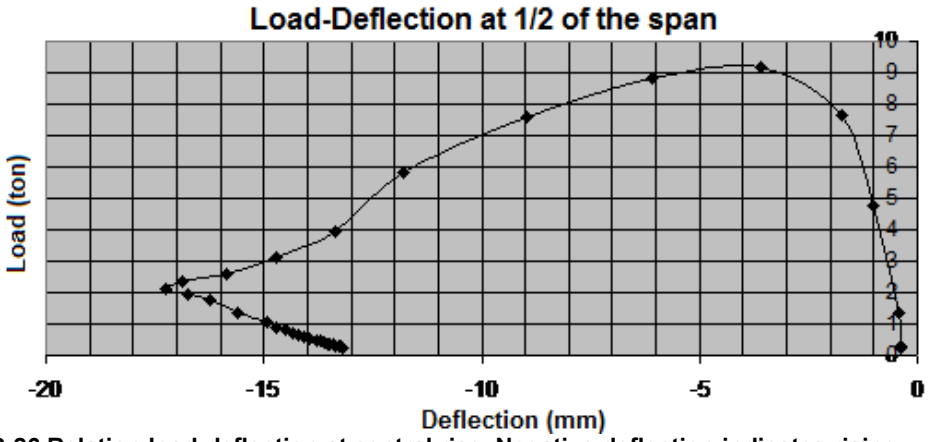

Figure 3-26 Relation load-deflection at central rise. Negative deflection indicates rising.

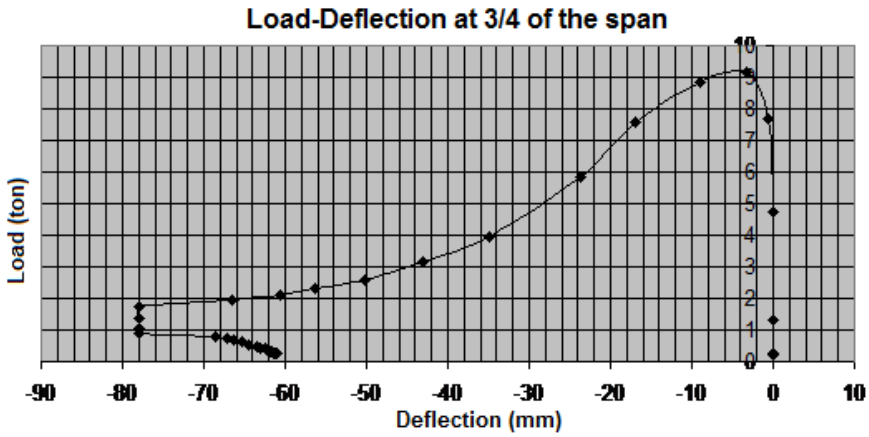

Figure 3-27 Relation load-deflection at the point symmetrical to the point of load application.

The largest displacements occur under at the point under the load and the point symmetrical to it with respect to the key. Moreover it is obvious, that under load the vertical displacements are indicating declining of the structure, while from center rise and on, the structure is rising.

The first transducer to detect deflections was located under the load. Figure 3-25 shows a change in the slope of the graph for a load value of 1tone. This could indicate the generation or development of the hinge, or the separation of the ring from the spandrel walls.

In fact, for the same value of load displacements started to be recorded by the strain gauge under the key. This could indicate that at this moment began the formation of the second and third hinge. However, this is an hypothesis that can not be assured, because as already said is impossible to establish a rigorous relationship between levels of damage and load.

The transducer at the point at ¾ of the span no deflections were registered until about 6 tons. In Figure 3-27 a change in slope is clear for approximately 7.6tons, which is also identified in the data taken at the point under the load and in the central rise. From that point the rate of deformation increases in the three transducers, which clearly indicates the formation of the fourth plastic hinge and therefore the collapse mechanism, is complete. What is interesting about this observation is that displacements in the point symmetrical to the loading point were not noticeable until the collapse mechanism was almost complete.

Once formed the collapse mechanism, despite the lowering of the load that the bridge had undergone, the displacements increased rapidly (a fact which confirms the formation of the four plastic hinges). The highest vertical displacements were recorded in the point at ¾ of the bridge's span (about 78mm upwards), followed by the point under the load (34 to 35 mm downwards) and, finally, in the center rise (about 17mm. upward).

The following three figures show the evolution of the deflections with the load during the execution of the second loading cycle.

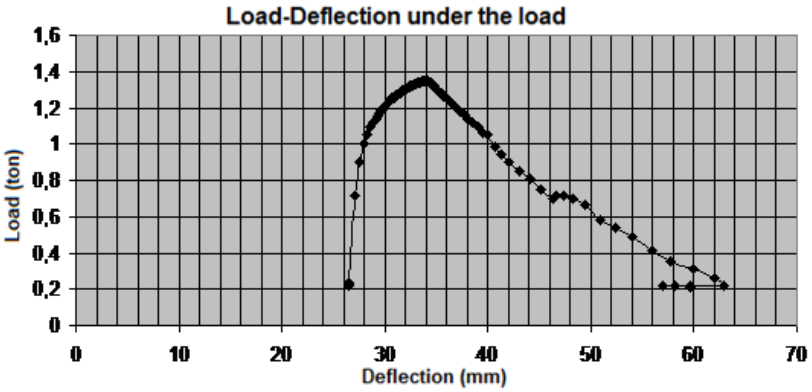

Figure 3-28 Load-displacement relationship at the point under the load for the second loading cycle

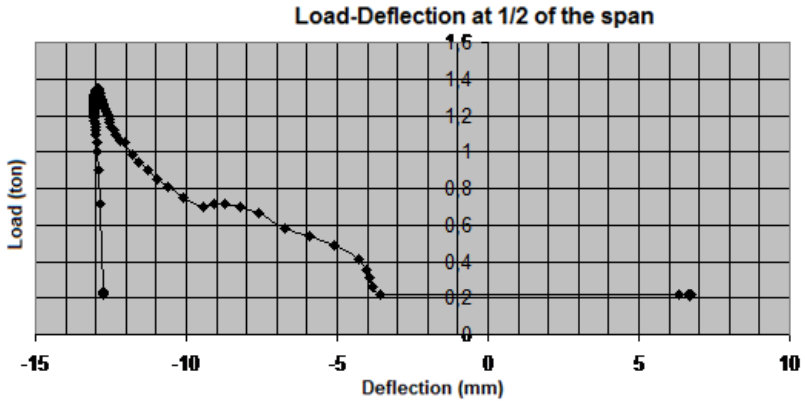

Figure 3-29 Load-displacement relationship in the central rise for the second loading cycle.

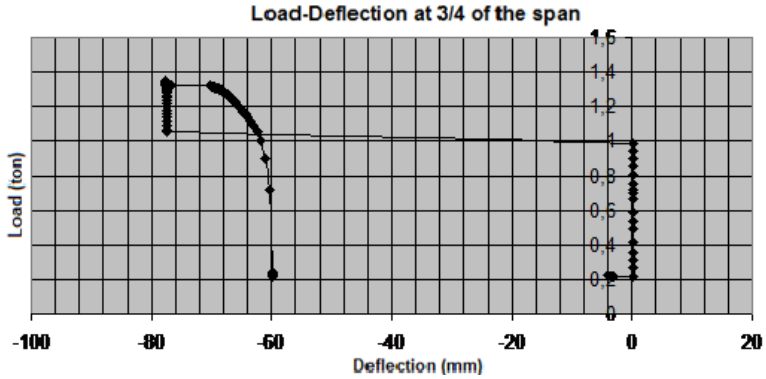

Figure 3-30 Load-displacement relationship in the point at ¾ of the bridge's span for the second charge cycle.

At the point under the load application and its symmetrical, it seems evident that the vertical displacement increases sharply from load of 1 ton, but at the central rise practically no displacement is observed. This indicates the possible rotation of a section of the arch between the two main hinges with respect to the key.

Soon after, and before reaching 1.4 tons, there is a sharp drop of the load in the three graphs. That point represents the time when the structure begins to yield. This seems to be the moment that the structure starts to collapse. The point under the load continues to fall, while the point at the central rise presented a sudden change of behavior, from ascending to descending, which clearly indicates the beginning of the collapse of the structure.

3.5.3 Limit analysis

Before performing a finite element analysis, a limit analysis was conducted in order to estimate a lower bound of the ultimate load carrying capacity and the configuration of the collapse mechanism of the masonry arch bridge. The analytical program Ring 2.0, which uses computational limit analysis methods to analyze the collapse state, was used for this purpose.

When using Ring 2.0 for a limit analysis, the structure is divided into a large number of discrete rigid blocks connected by zero thickness and zero tensile strength joints. The program has the capacity to simulate the masonry arch ring, the backing and the backfill, but does not take into account the contribution of the spandrel walls to the total capacity of the bridge.

In the geometry dialog of the program, the intrados shape was defined as segmental and the voussoir type as brick bonded, while 86 masonry units were considered along the ring. The dimensions in mm for all the parts of the bridge are shown in Table 3-4.

Bridge width	Span	Rise at midspan	Ring thickness	Backing Height	Pier Height	Pier Width (Top)	Pier Width (Base)
1000	3200	1600	140	810	170	1000	1000

Table 3-4 Bridge dimensions

For the fill profile, taking the springer of the arch as the origin, the x and y co-ordinates at a point on the lower edge of the surface fill are 4200mm and 1850mm respectively.

As far as the masonry properties are concerned, the unit weight was specified to be 18kN/m^3 and crushing was modeled, considering the compressive strength equal to 14N/mm^2. Also potential sliding between blocks, both within piers and rings and between adjacent rings, as well as sliding between all blocks was taken into account by defining a standard coefficient of friction equal to 0.6 and an inter-ring coefficient of friction equal to 0.5.

The backfill properties are presented in Table 3-5.

Soil properties			Live load dispersion details		Soil-arch interface properties		Passive zone parameters	
Unit weight (kN/m^3)	Angle of friction φ (degrees)	Cohesion c (kN/m^2)	Type	Cutoff Angle (degrees)	Friction multiplier on φ	Adhesion, multiplier on c	Factor m_p	Factor m_{pc}
18	38	0	Uniform	0	0.66	0.5	0.33	0.01

Table 3-5 Backfill properties

It is important to note that the uniform live load dispersion was selected to specify that the magnitude of the pressure exerted on the back of the arch is to be constant. The length of arch assumed to be subject to vertical loading pressures is controlled by the specified cutoff angle as indicated Figure 3-31.

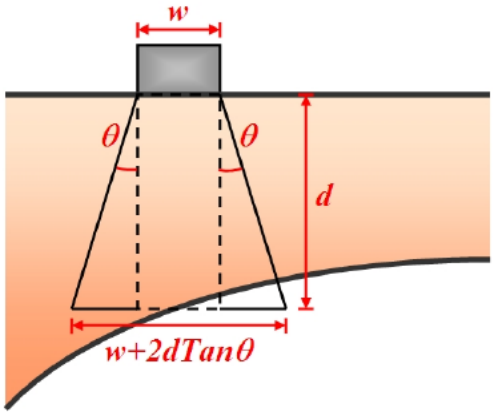

Figure 3-31 Uniform live load dispersion

Finally, an axle of 720mm width, 200mm loaded length and 1kN load, was positioned in 1/4th of the span and the abutments were constrained as fixed.

The failure load resulted from the analysis was 16.5281kN (16.5285kN for c=0.02kN/m^2) and the associated failure mechanism involved four hinges located over the backing height. The failure mechanism as well as the thrust line is shown in Figure 3-32.

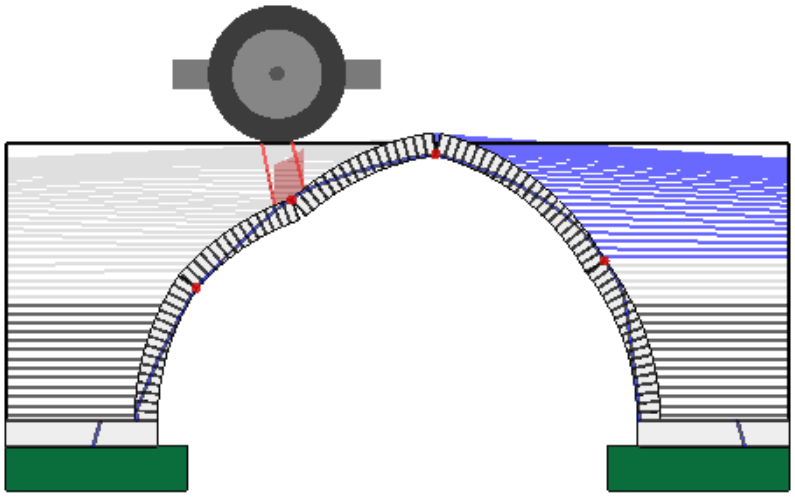

Figure 3-32 Failure mechanism

The first hinge is located at the intrados at x=234mm and the second one at the extrados at x=896mm approximately under the applied load. The third and fourth hinge are located symmetric locations at the intrados at x=1855mm and at the extrados at x=2976mm respectively (the coordinate system is positioned at the left hand intrados springing).

The difference between the actual ultimate load which emerged from the experimental procedure and the one obtained from the limit analysis is due to several factors. One very important factor which is not taken into account is the beneficial contribution of the spandrel walls in the ultimate strength of the structure. It has to be mentioned that the width of the spandrel walls is almost 1/3rd of the width of the bridge. Also the selection of the type of live load dispersion as well as the cutoff angle, are of great importance and might lead to different results.

It has been observed that by differentiating the variables available by Ring 2.0, looking for the ultimate load, small changes in the assumptions and parameters during modeling the bridge lead to significant changes in the value of the ultimate load. Thus a careful selection of all the factors before running the analysis is of great importance.

4. PLANE STRESS FINITE ELEMENT ANALYSES OF THE MASONRY ARCH BRIDGE

4.1 Introduction

Before moving to a more complex analysis of a 3D finite element model of the masonry arch bridge, it was considered necessary to create a plane stress model. This type of model is much simpler, so that the analysis and the elaboration of the results is much less time consuming. Thus, by using this model we had the opportunity to perform a small sensitivity analysis in order to identify the influence of each parameter to the behaviour of the bridge and to select the appropriate and more realistic material models, which are capable to describe the behaviour and the failure mechanism of the structure.

Firstly, we ran a linear analysis in order to verify that the model was working properly and then ran a number of non-linear analyses focusing in the influence of one property each time. The FEM calculations were carried out by the FE program DIANA 9.4 which provides all the necessary non-linear constitutive models for the materials.

4.2 General assumptions

Given the fact that a plane stress model is a 2D model, some basic assumptions should be done before modelling. Thus, the spandrel walls were totally disregarded and the bridge was supposed to be composed by the concrete abutments, the soil infill, the masonry arch ring and the backing, which was assumed to be made of masonry with the same properties as the ring. Furthermore, even thought the spandrel walls were not to be modelled, we decided to set the width of the bridge equal to 1m.

Moreover, the bridge was supposed to be fixed-ended under the concrete slabs and in the cases that the bracing system was not modelled, the x displacement was constrained in the right and left side of the structure. In the cases that the bracing system was taken into account, it was supposed to be composed of two steel plates of 2cm thick attached to each side of the bridge and connected with each other by 4 ties with cross-section of 981.75mm^2. We used ties this cross-section trying to simulate the actual structure in which there were 4 ties in the front side and 4 ties in the back side with diameter of 25mm each (cross-section of 490.87mm^2).

Friction interface elements were introduced between the arch ring and the filling in order to simulate possible relative slipping between the two.

Finally, it has to be noted that all the concrete and the steel elements have linear properties for all the analyses and that in order not to apply the load directly on the infill, a concrete beam was positioned at ¼ of the span of the bridge with cross-section of 200x200mm. The load was applied as pressure distributed on the upper side of this beam.

4.3 Numerical modelling of the masonry arch bridge

After creating the geometry of the structure in Autocad, the model was introduced in DIANA 9.4. The first thing to be done was to define the units (mm, N, kg) and then the generation of the surfaces and the meshing. The plane stress and interface elements used for the meshing are listed and described below:

- Plane stress element Q8MEM: The Q8MEM element [Fig. 4-1] is a four-node quadrilateral isoparametric plane stress element. It is based on linear interpolation and Gauss integration.

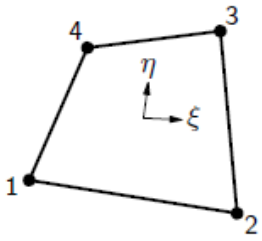

Figure 4- 1 Q8MEM

- Plane stress element T6MEM: The T6MEM element [Fig. 4-2] is a three-node triangular isoparametric plane stress element. It is based on linear interpolation and area integration. This element was used only for some triangular surfaces.

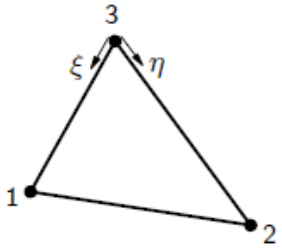

Figure 4- 2 T6MEM

- Interface element L81F: The L8IF element is an interface element between two lines in a two-dimensional configuration [Fig. 4-3]. The element is based on linear interpolation.

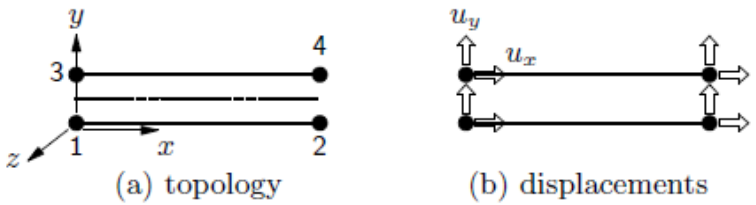

Figure 4- 3 L81F

- Truss element L2TRU:

The L2TRU element [Fig. 4-4] is a two-node directly integrated (1-point) truss element which may be used in one-, two-, and three-dimensional models.

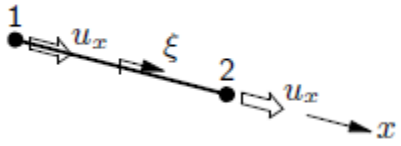

Figure 4- 4 L2TRU

It has to be mentioned that the mesh on the ring is denser near the intrados and the extrados (Figure 4-5) in order to avoid stress concentration at the points where the hinges are to be formatted.

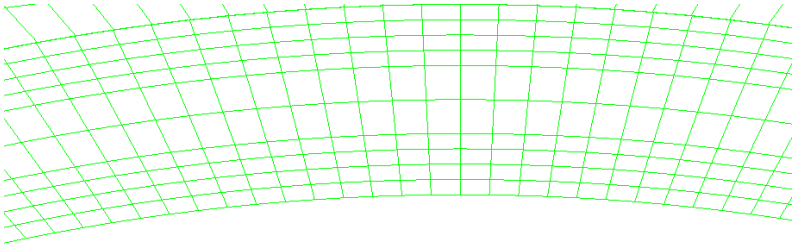

Figure 4- 5 Meshing in the arch ring

The mesh configuration is shown in Figure 4-6. The number of the nodes and the elements generated in total is 5543 and 5327 correspondingly.

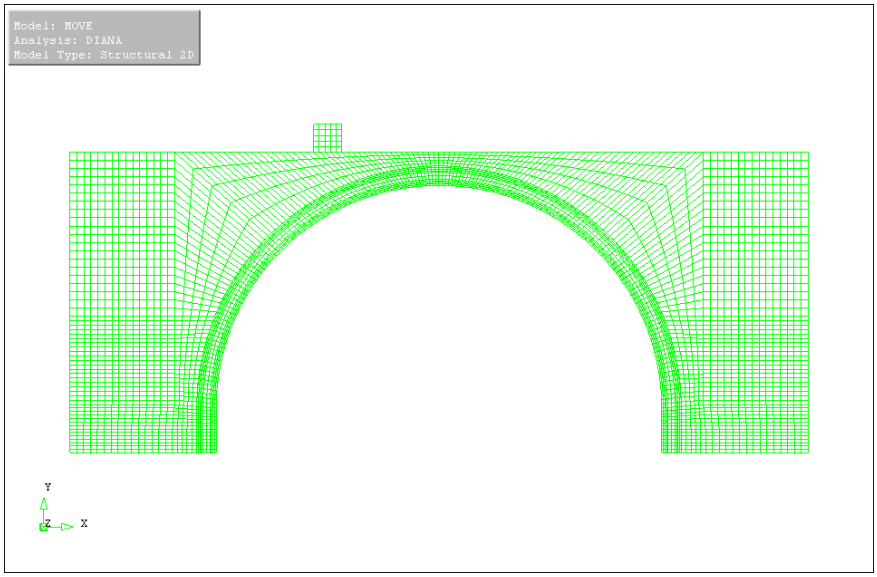

Figure 4- 6 FEM meshing

After the mesh generation, we defined the width of the structure equal to 1m and the material properties as they are described in the next sections. The material distribution on the model is shown in Figure 4-7. The final step was the definition of the constraints as explained before and the application of the loads (self-weights and pressure on the concrete beam).

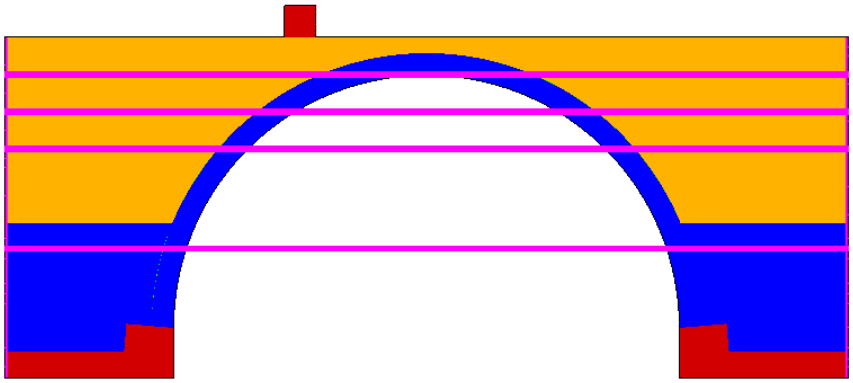

Figure 4- 7 Materials distribution on the model (red=concrete, blue=masonry, yellow=soil, magenda=steel).

4.4 Linear analysis

The material properties used for the linear analysis are listed below (it has to be mentioned that the following properties of concrete are the ones used for all the analyses presented later):

Property	Concrete	Masonry	Soil	Interfaces
Young's Modulus	34000 N/mm^2	5500 N/mm^2	37.76 N/mm^2	—
Poisson's ratio	0.15	0.18	0.2	—
Mass density	2.4e-06 kg/mm^3	1.8e-06 kg/mm^3	1.8e-06 kg/mm^3	—
Linear normal stiffness	—	—	—	1e+06 N/mm
Linear tangential stiffness	—	—	—	1e+06 N/mm

Table 4- 1 Material properties for the linear analysis

The load applied on the linear model was 17kN. In the next pictures are presented the results of the linear analysis.

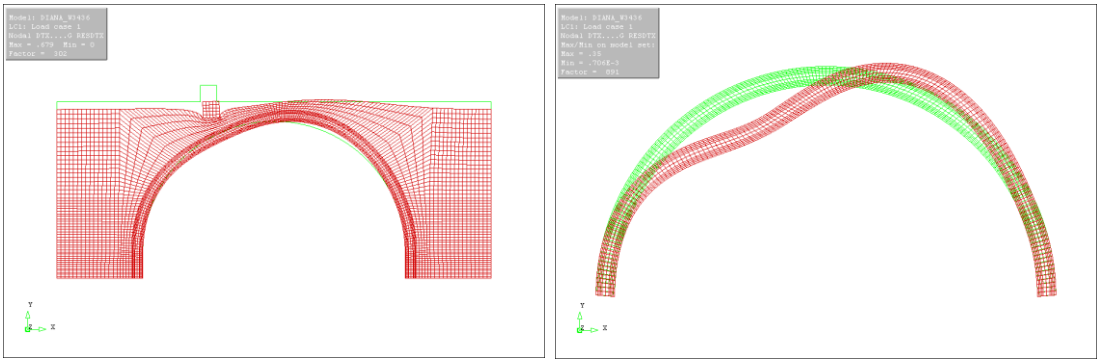

Figure 4- 8 Deformed shape of the structure. Deformed shape of the arch ring.

As Figure 4-8 depicts, the maximum displacements are located in the area under the load application where the structure is descending in contrast to the area on the right of the key where as expected the structure is rising.

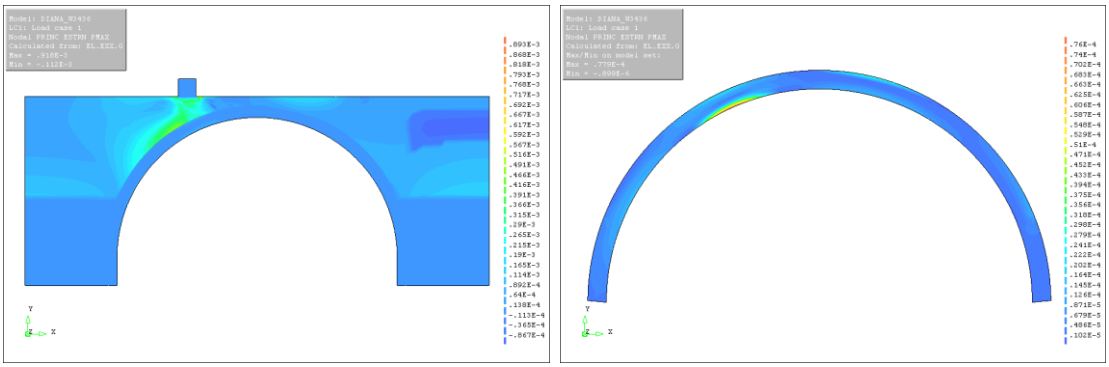

Figure 4- 9 Maximum principal strains.

From the principal maximum strains (Figure 4-9) we can see the load dispersion through the soil and also higher strains at ½ and ¾ of the bridge's span, location where two of the four hinges are to be generated.

Beyond these preliminary conclusions, the linear analysis cannot provide us sufficient results regarding the ultimate load and the formation of the collapse mechanism. Thus, the non-linear analysis of the structure is of great importance.

4.5 Non-Linear analyses

A number of non-linear analyses were performed in order to determine the appropriate constitutive models and parameters which best describe each material. Moreover trials have been performed with and without the bracing system to figure out its contribution to the ultimate load and the configuration of the collapse mechanism.

Finally, trying to simulate in a better way the behavior of the soil, we created a second model. The soil's elasticity modulus is not constant. It is increased with the depth. Thus, for the second model we created 5 different layers of soil of approximately 235mm of height each.

4.5.1 Non-linear analyses with one layer of soil

4.5.1.1 Non linear analysis without the bracing system

After several trials we reached the material properties listed below which describes the behavior of each material in the best possible way. The concrete properties are the same as in section 4.4.

- **Soil:** The Mohr-Coulomb plasticity model was used to describe the soil. The parameters used are the following:

Young's modulus: 37.76 N/mm^2 (we used the formula E=0.32*z (MPa) for the maximum depth, where z is the depth in cm)

Poisson's ratio: 0.2

Mass density: 1.8e-06 kg/mm^3

Cohesion c: 0.018 N/mm^2 (The minimum value for which we achieved convergence. It has to be noted that the smaller the cohesion, the bigger the strains on the arch ring).

Friction angle: 38^o

Dilatancy angle: 38^o

- **Masonry:** The energy based total strain fixed crack model was used for the masonry. The tensile behavior is described of linear softening, while the compression curve is of parabolic shape (Figure 4-10).

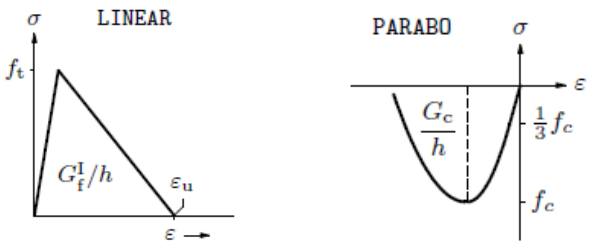

Figure 4- 10 Linear softening in tension. Parabolic diagram in compression

The parameters used are:

Young's modulus: 5500 N/mm^2

Poisson's ratio: 0.18

Mass density: 1.8e-06 kg/mm^3

Tensile strength: 0.05 N/mm^2

Compressive strength: 14N/mm^2

Tensile fracture energy: 0.03 Nmm^{-1}

Compressive fracture energy: 5 Nmm^{-1}

Shear retention factor: 0.01

- **Interfaces:** a simple frictional contact surface for the soil-arch interface with no hardening has been assumed. The properties considered are:

Linear normal stiffness: 1e+06 N/mm

Linear tangential stiffness: 1e+06 N/mm

Cohesion: 0.04 N/mm^2 (The minimum value for which we achieved convergence).

Friction angle: 38^o

Dilatancy angle: 38^o

The load was divided into two load cases. The first one is the self-weight and the second one is the live load of 17kN applied in ¼ of the span of the bridge.

For the non linear analyses, arc length control with reference one of the points where the live load is applied was used and the convergence criteria, are the following:

- Maximum number of iterations:50
- Abort criterion for energy, displacement and force: 10^{10}
- Convergence tolerance:0.0001
- Steps for LC1: 0.5 (20)
- Steps for LC2: 0.005 (215)

The maximum load achieved from the analysis was 17.85kN which is obviously much lower than the actual failure load, but this was something expected since the contribution of the spandrel walls, which are almost 1/3 of the bridge's width, is disregarded in the analysis.

Moreover, the ultimate load calculated from the plane stress model analysis is higher than the one calculated using the limit analysis program Ring 2.0. This was also something that we were expecting since one of the basic assumptions of the limit analysis is that the masonry has no tensile strength in contrast to the finite element analysis performed for which we defined the tensile strength equal to 0.05 N/mm^2.

Figure 4-11 depicts the deformed shape of the structure and the ring in the final load step. The maximum displacement of the structure is 1.39mm and is located on the concrete beam on which the load is applied. On the ring, the maximum displacement is 0.475mm located under the area where the load is applied.

Finally we have to note that the deformed shape fits the failure mechanism of the structure as it was described in previous section. The hinges seem to appear under the load application, to its symmetrical point with respect to the key and at the points near the two abutments.

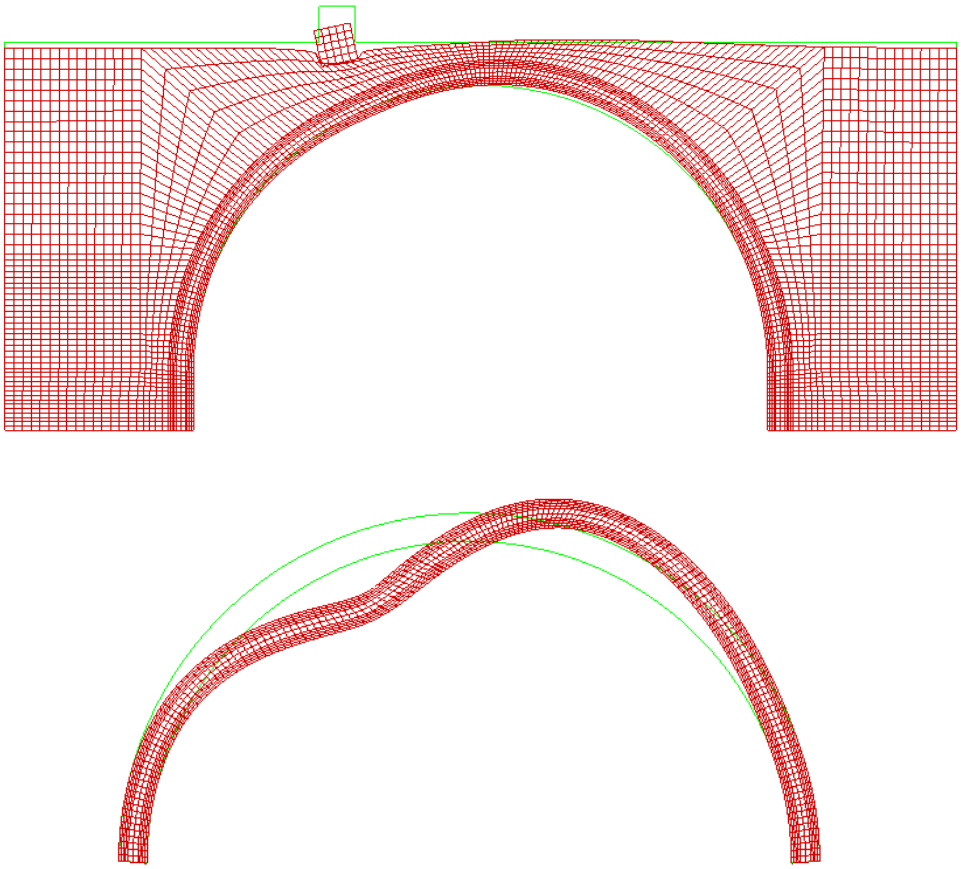

Figure 4- 11 Deformed shape of the structure and the arch

The load-vertical displacement graphs for one of the nodes on the ring intrados under the load application and one of the nodes on the ring extrados in position symmetrical to the load application with respect to the key are shown in picture 4-12. The behavior is almost linear until load factor of 0.4 (approximately 7kN) under the load and of 0.5 (8.5kN) at ¾ of the bridge's span and then it becomes non-linear.

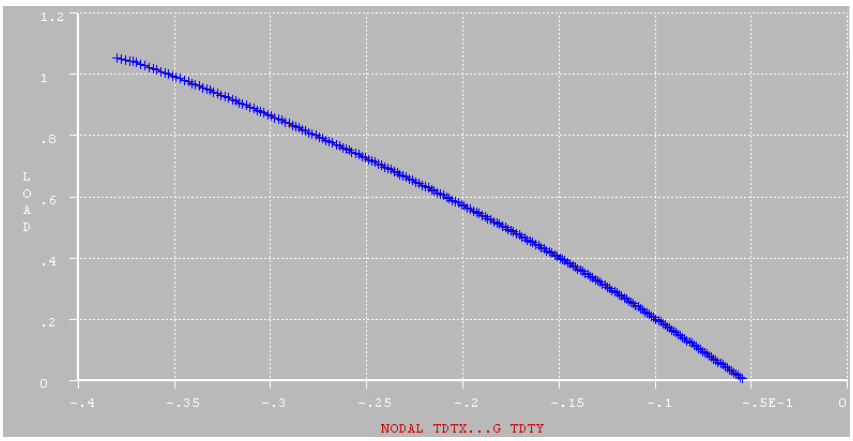

(a)

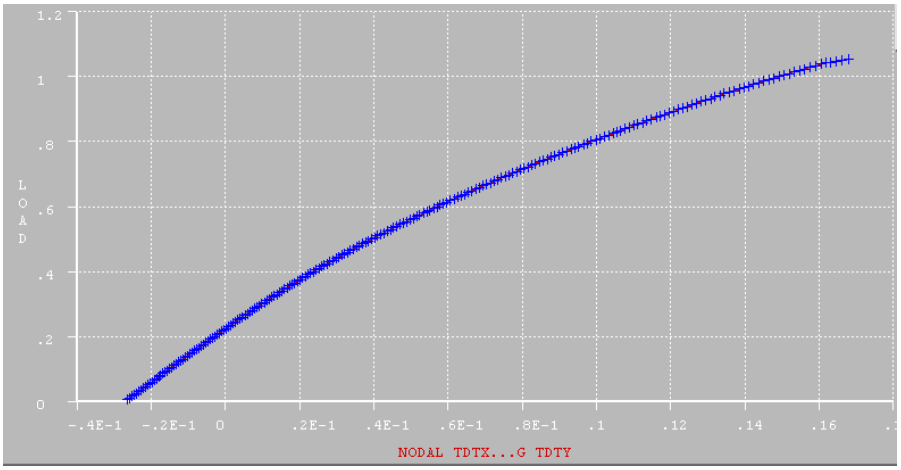

(b)

Figure 4- 12 (a) load-vertical displacement graph under the load. (b) load-vertical displacement graph at ¾ of the span

The maximum principal strains calculated from e_{xx} are presented in the next figure for the whole structure and for the masonry ring again for a total load of 17.85kN. In figure 4-13 (a) the greater distribution of strains over the soil is obvious, while in figure 4-13 (b) we can see strain concentration on the areas that the generation of hinges was expected. Three out of four hinges seem to be completely formatted. The maximum principal strain on the ring is 4.42e-2 mm/mm and on the whole structure 0.0836mm/mm.

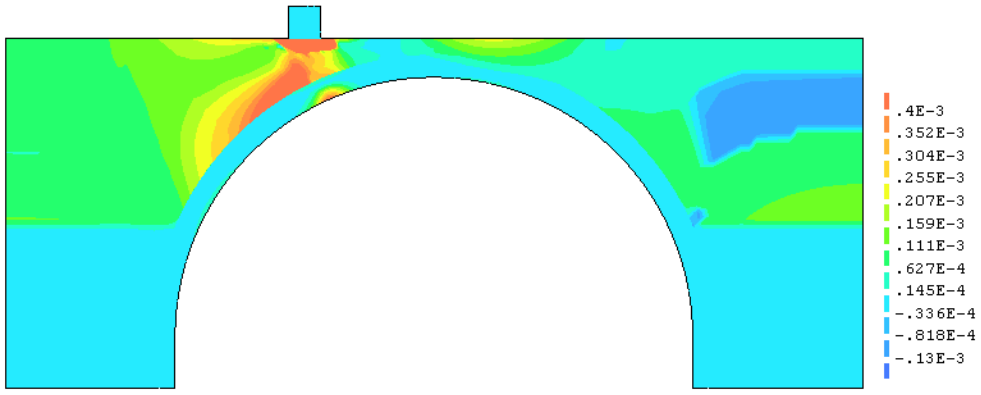

(a)

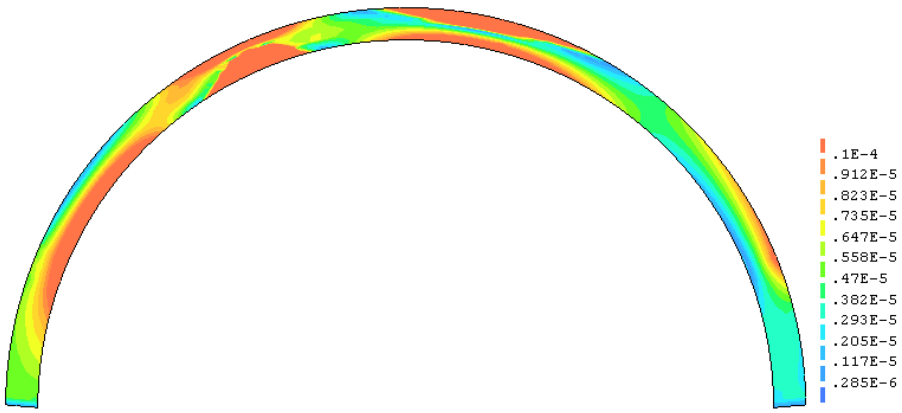

(b)

Figure 4- 13 Principal strain distribution

Finally the following figures depict the maximum, minimum principal stresses and Von mises stresses calculated from s_{xx} on the ring.

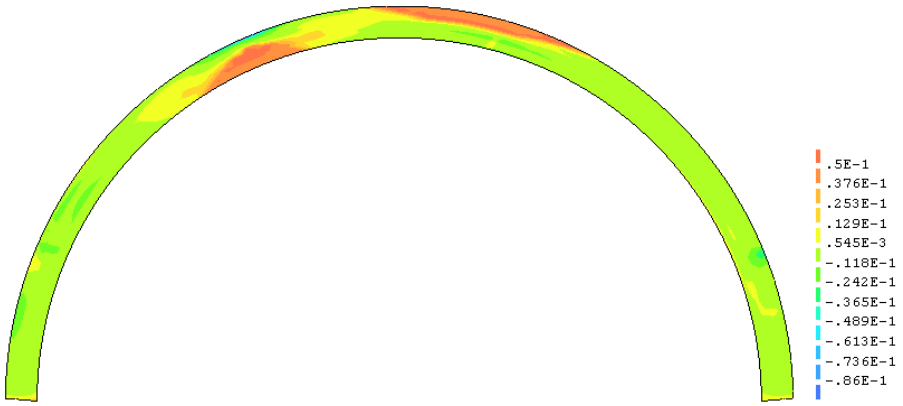

Figure 4- 14 Maximum principal stresses calculated from s_{xx} (P_{1max}=0.0654MPa, P_{1min}=-0.0862 MPa)

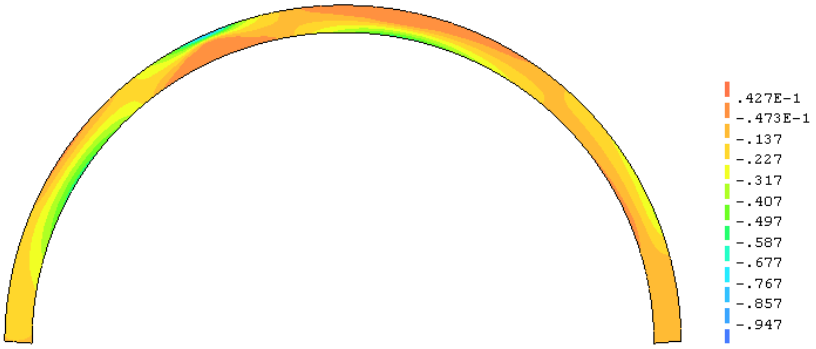

Figure 4- 15 Minimum principal stresses calculated from s_{xx}(P_{2max}=00.0427MPa, P_{2min}=-0.947 MPa)

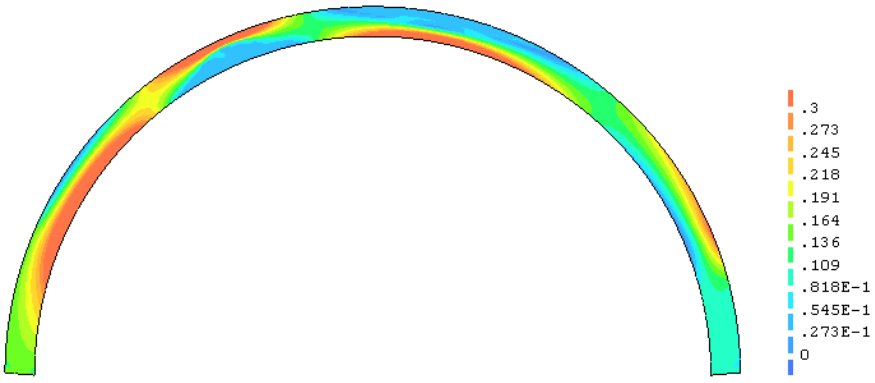

Figure 4- 16 Von mises stresses calculated from s_{xx}(P_{vmmax}=0.91MPa, P_{vmmin}=0.311e-2MPa)

It seems that two out of four hinges are fully formatted (stresses over the tensile strength of the masonry). The other two can be distinguished but are not fully formatted.

4.5.1.2 Non linear analysis with the bracing system

As mentioned before the bracing system was simulated by two steel plates of 2cm thick attached in the right and left sides of the bridge and connected with each other with 4 bars with cross-section of 981.75mm^2.

The material properties are the same as in section 4.5.1.1 and the properies used for the steel of the bracing system are:

- **Steel:** linear elastic properties

Young's modulus: 210000 N/mm^2

Poisson's ratio: 0.3

Mass density: 7.85e-06 kg/mm^3

The ultimate load reached from this analysis is slightly bigger than before and equal to 18.02kN.

Figure 4.17 shows the deformed shape of the structure and the arch. The maximum displacement is 4.92mm located on the concrete beam and the maximum displacement of the arch is 0.579mm again located under the load. This means that the maximum displacement on the bridge is 3mm more than in the previous analysis.

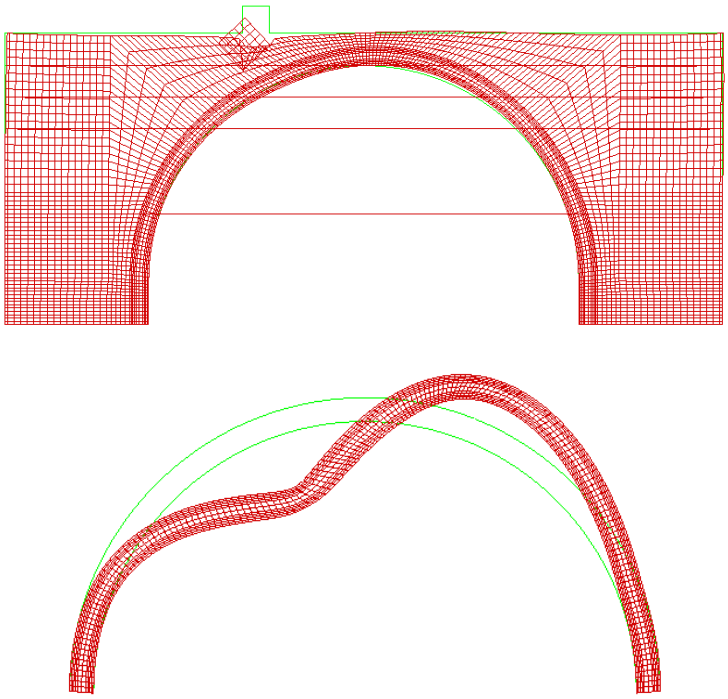

Figure 4- 17 Deformed shape of the structure and the arch

The next pictures show the graph of load-vertical displacement for one of the nodes on the intrados of the ring under the load and one of the nodes on the extrados in symmetrical position. A linear area is distinguished in the beginning of the graphs until a load factor of

approximately 0.4 (6.8kN) for the first graph and 0.42 (7.14kN) for the second one. Then the graph becomes nonlinear and close to the ultimate load becomes constant which indicates plastification.

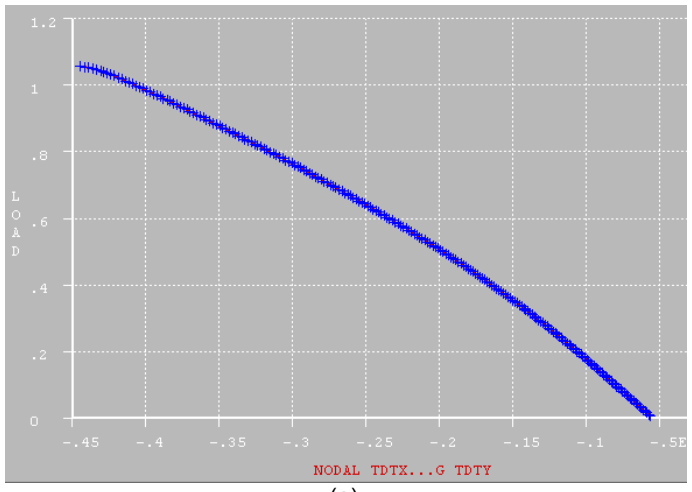

(a)

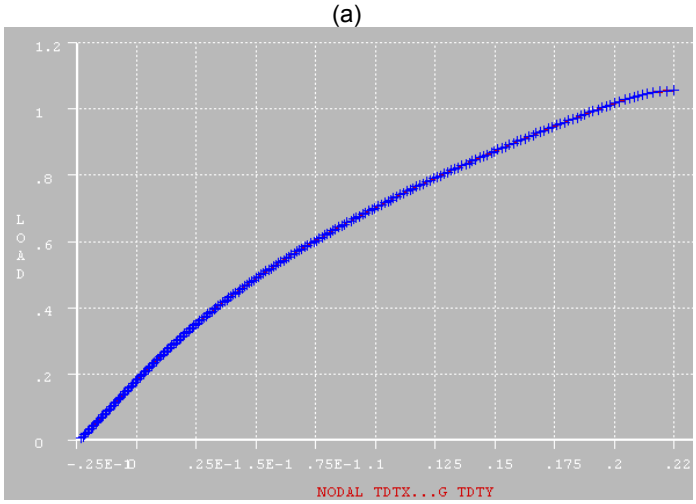

(b)

Figure 4- 18 Load-vertical displacement graph on the (a) intrados of the arch ring under the load and (b) on the extrados symmetrically to the load

In figure 4-19, we can see the maximum principal strain calculated from e_{xx}. In this case the maximum principal stresses are bigger. The maximum principal strain on the ring is 5.67e-2 mm/mm and on the whole structure 0.101mm/mm.

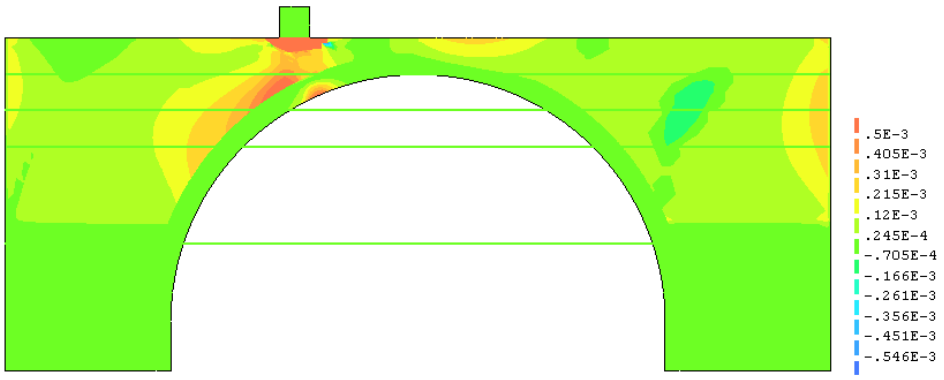

(a)

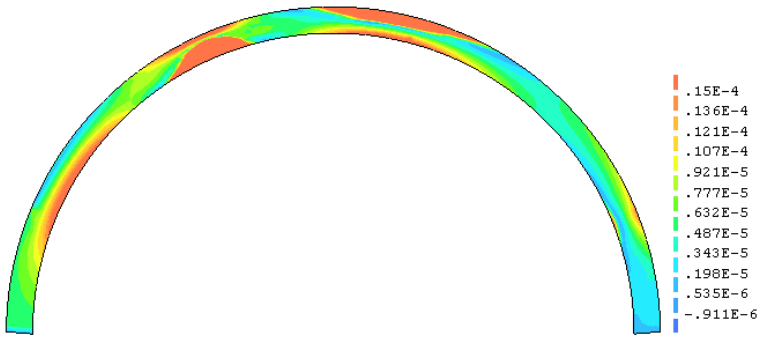

(b)

Figure 4- 19 Maximum principal strains calculated from e_{xx}

Once again, in the next figures we present the maximum, minimum principal stresses and the Von mises stresses calculated from s_{xx} on the ring and the whole structure. We have to note that part of the tensile stresses is undertaken by the ties which also transfer stresses to the steel plates (Figure 4-20). About 1.07Mpa are undertaken from the first tie and 1.04Mpa from the third one.

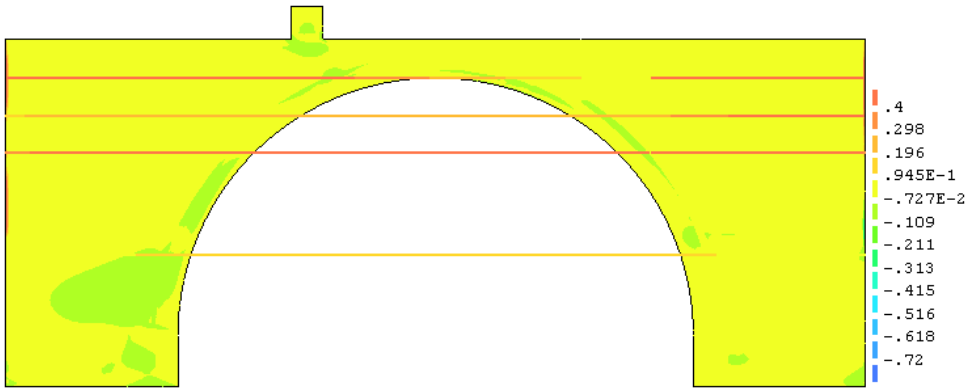

Figure 4- 20 Maximum principal stresses calculated from s_{xx} (P_{1max}=1.86 MPa, P_{1min}=-0.72 MPa)

Figure 4- 21 Maximum principal stresses calculated from s_{xx} (P_{1max}=0.0742MPa, P_{1min}=-0.0928 MPa)

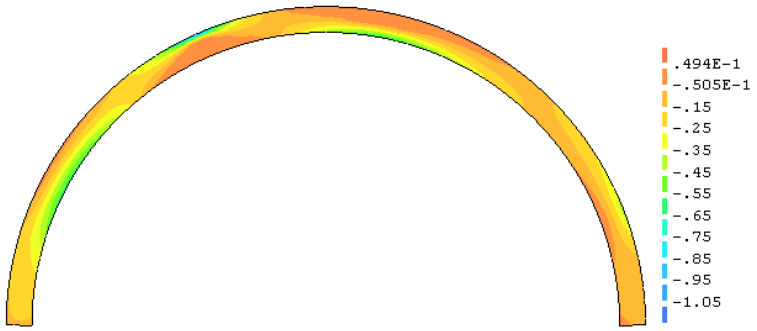

Figure 4- 22 Minimum principal stresses calculated from s_{xx}(P_{2max}=0.0494MPa, P_{2min}=-1.05 MPa)

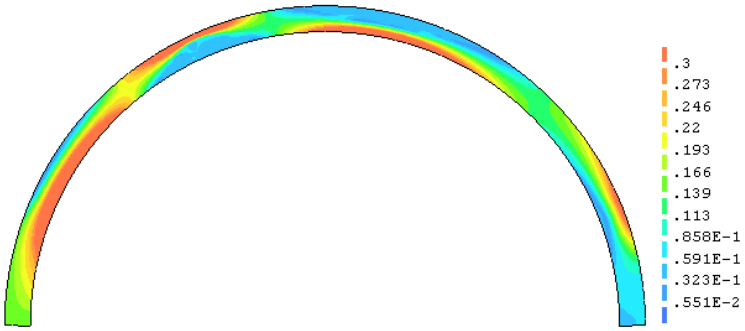

Figure 4- 23 Von mises stresses calculated from s_{xx}(P_{vmmax}=1.01MPa, P_{vmmin}=0.551e-2MPa)

Even thought the stresses are higher than in the previous analysis, the collapse mechanism is still not clear. Two out of the four hinges are obvious and the other two seem to develop (only a small area of the ring presents tensile stresses over the tensile strength of the masonry).

4.5.2 Non-linear analysis with several soil layers and bracing system

In order to optimize the results of our study, we decided to create a new model in order to reach a more realistic behavior of the soil and consequently of the structure itself. In the new model, the soil is composed of five layers of different Young's modulus each (Figure4-24). The formula used for the calculation of the Young's modulus of each layer is E=0.32*z (MPa), where z(cm) is the average depth of each layer. The resulting values are listed in table 4-2.

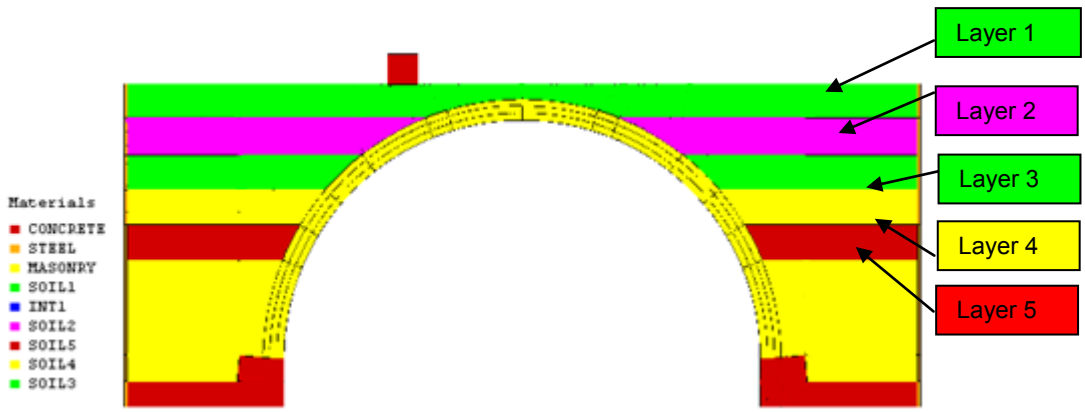

Figure 4- 24 Soil layers positions on the model

Soil layer	Young's modulus (MPa)
1	3.61
2	11.16
3	18.88
4	26.43
5	33.98

Table 4- 2 Young's modulus values for each soil layer

The rest of the material properties and all the assumptions are the same as in the previous sections.

The maximum load factor reached was 1.04 on the applied load of 17kN, which corresponds to 17.68kN. For this load, the deformed shape of the structure and the ring is shown in Figure 4-25. The maximum displacement on the ring is 0.99mm and on the whole structure 2.75cm.

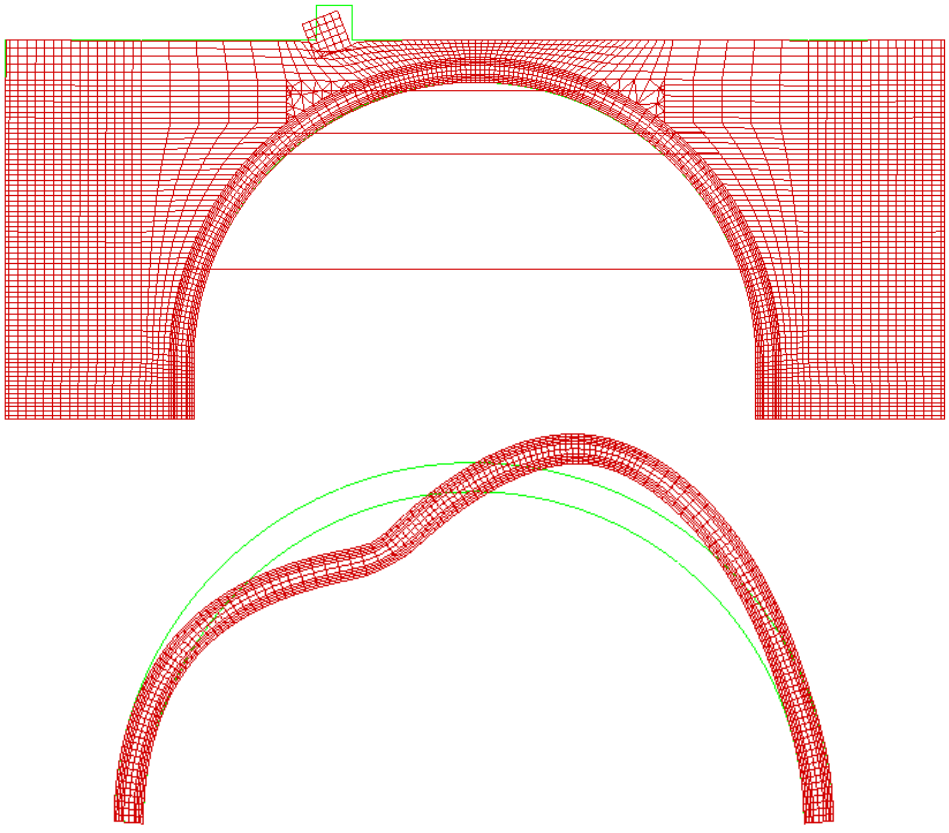

Figure 4- 25 Deformed shape of the structure and the ring for load of 17.68kN

In the following figures, the load-vertical displacement graphs for two nodes. The first one is located on the intrados of the arch ring under the load and the second on the extrados symmetrically to the first one. Negative values correspond to descending of the structure, while the positive ones indicate rising.

The point under the load (Figure 4-26) is descending. The graph is linear in the first part until load factor of approximately 0.3 (5.1kN) and then becomes nonlinear. The last part of the graph is constant that indicates plastification of the material in this area.

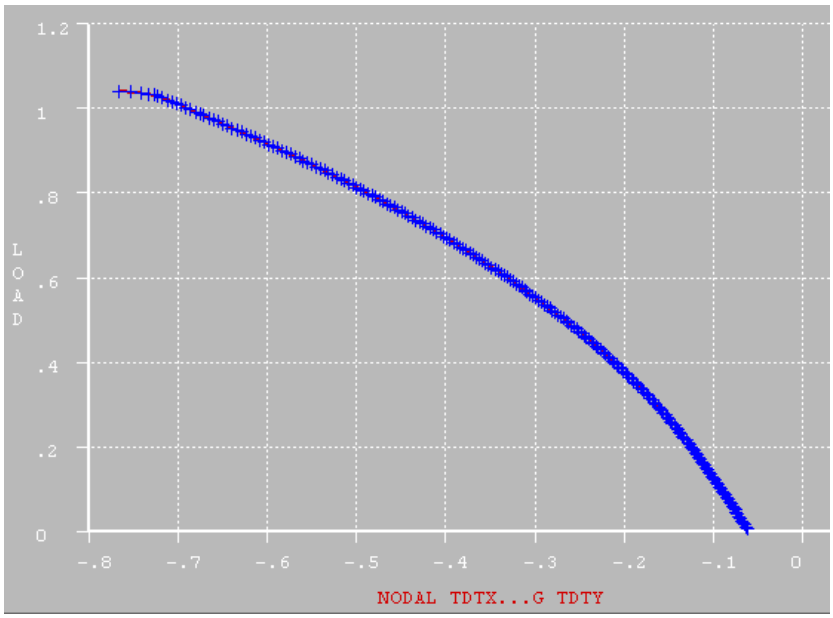

Figure 4- 26 Load-vertical displacement graph on the intrados of the arch ring under the load

In figure 4-27 we can see that the point on the extrados at approximately ¾ of the arch's span is rising in a linear way until load factor of 0.4 (6.8kN) and from that point on in a nonlinear way. Again in the final load steps, the material is plasticized.

From these two figures we can presume that the hinge under the load is the first to be generated.

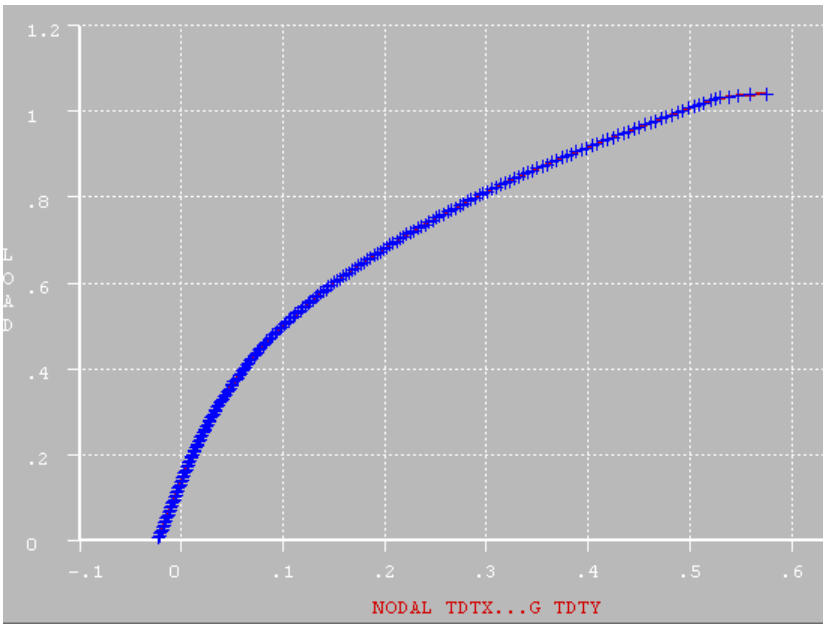

Figure 4- 27 Load-vertical displacement graph on the extrados symmetrically to the point of load application

The maximum principal strains, calculated from e_{xx}, on the arch ring are presented in Figure 4-28. The maximum value is P_{1max}=0.142e-2mm/mm. From the strains configuration it is easy to identify the location of the four plastic hinges of the collapse mechanism.

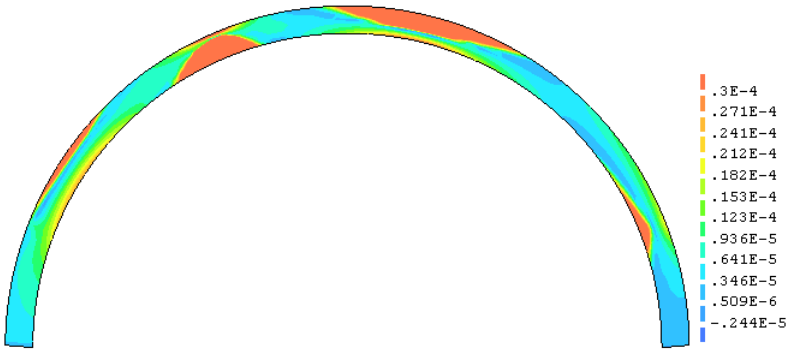

Figure 4- 28 Maximum principal strains on the arch ring.

the next figures depict the maximum, minimum principal stresses and the Von mises stresses calculated from s_{xx} on the ring and the whole structure. We have to note that again part of the tensile stresses is undertaken by the ties which in turn transfer stresses to the steel plates (Figure 4-29).

The maximum value of the maximum principal stresses on the bridge is 2.05MPa and on the ring 0.0744MPa.

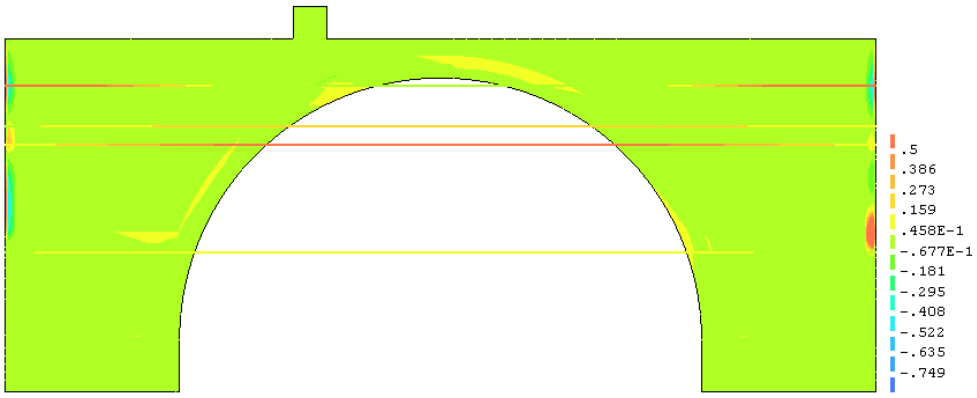

Figure 4- 29 Maximum principal stresses calculated from s_{xx} (P_{1max}=2.05MPa, P_{1min}=-0.749 MPa)

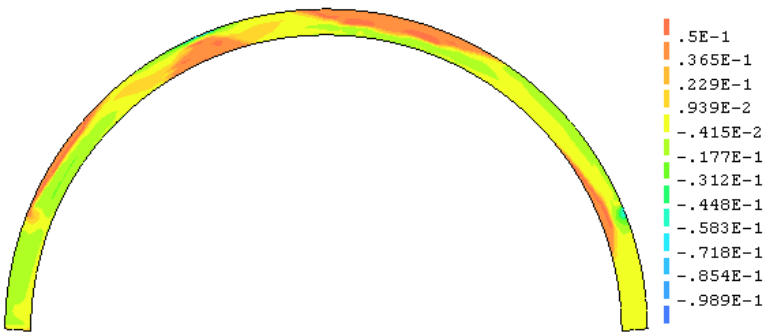

Figure 4- 30 Maximum principal stresses calculated from s_{xx} (P_{1max}=0.0744MPa, P_{1min}=-0.0989 MPa)

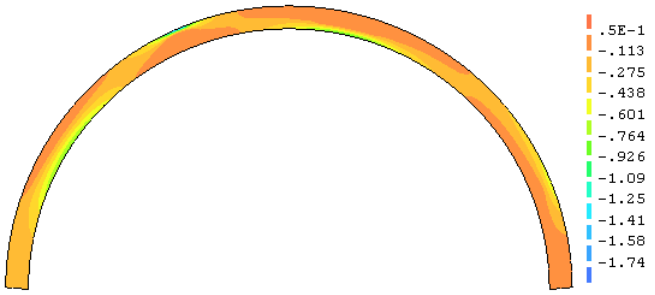

Figure 4- 31 Minimum principal stresses calculated from s_{xx}(P_{2max}=0.0505MPa, P_{2min}=-1.74 MPa)

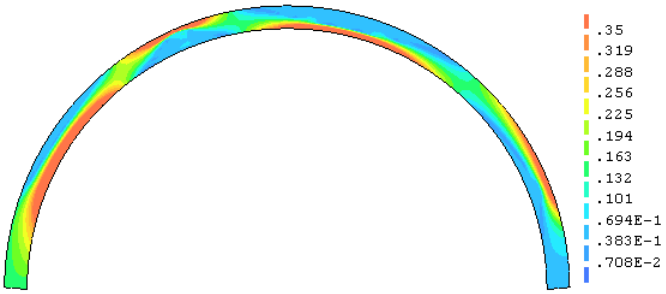

Figure 4- 32 Von mises stresses calculated from s_{xx}(P_{vmmax}=1.69MPa, P_{vmmin}=0.708e-2MPa)

This time the collapse mechanism of four plastic hinges is clear (in Figure 4-30 we can recognize the plastic hinges in the areas that the stress is over the tensile strength of the masonry). The locations of the hinges are the following:

- On the intrados under the load application
- On the extrados symmetrically to the load application
- On the extrados on the left of the load and near the abutment
- On the intrados on the right of the second hinge and near the right abutment.

4.5.3 Comparison between the three models and the experimental results

An easy way to compare the influence of the ties as well as the influence of dividing the soil filling into several layers is to compare the graphs of load-vertical displacement for each case. For the comparison we decided to use the graph for one of the nodes on the intrados of the arch under the load application.

In figure 4-33 we can see in the same graph the curves load-vertical displacement corresponding to model 1 (one layer of soil without the bracing system) and to model 2 (one layer of soil with the bracing system).

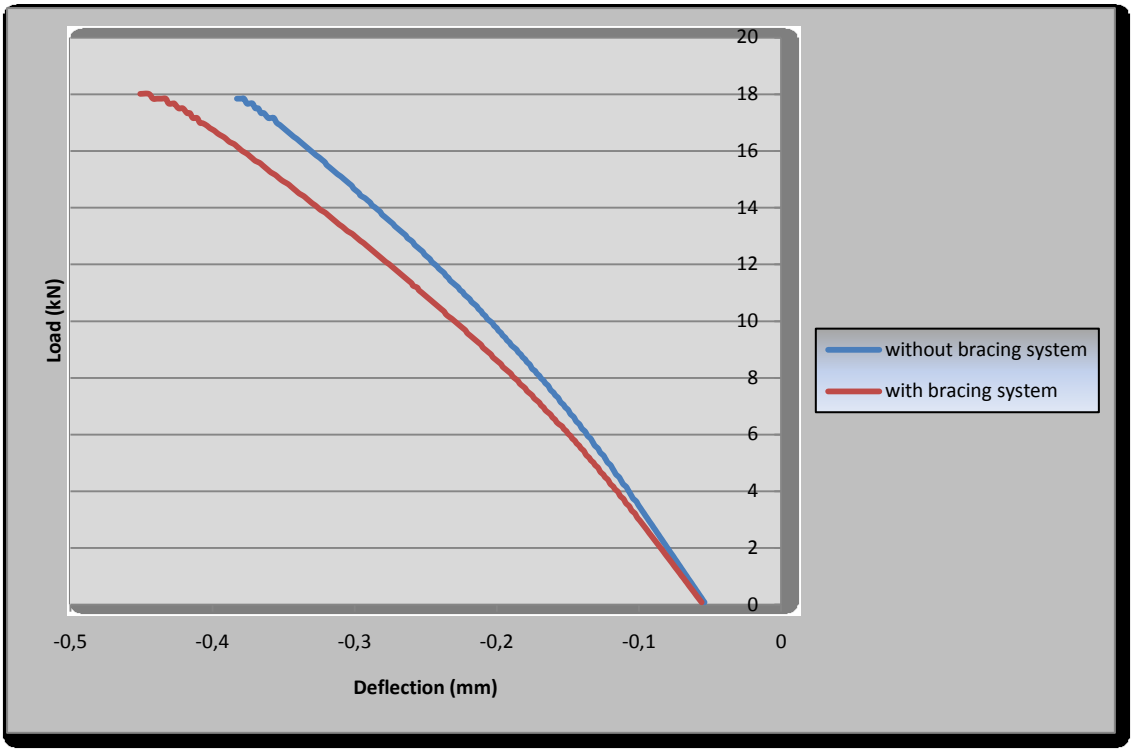

Figure 4- 33 Load-vertical displacement graph for one of the nodes on the intrados of the arch under the load application for model 1 and model 2

The inclination of the curve corresponding to the model without the bracing system is sharper. The displacements are smaller for each load step and the ultimate load reached is smaller than the one for the model with the bracing system. This leads us to the conclusion that simulating the bracing system instead of constraining the x displacements on the each side of the bridge, makes the structure less stiff, able to deform more until the ultimate load is reached.

Figure 4-34 shows in the same graph the curves load-vertical displacement corresponding to model 2 (one layer of soil with the bracing system) and to model 3 (five layers of soil with the bracing system). Once again the graphs are plotted for one of the nodes on the intrados of the arch under the load application.

In this case the inclination of the curve which corresponds to model 3 is smoother. The displacements for this model are bigger in each load step, but the ultimate load reached is smaller compared to model 2. This is because in the model in which we divided the soil into five layers, the Young's modulus used for each layer was smaller than the one used for model 2 and thus, the soil doesn't have the capacity to undertake the same stresses. The stresses are undertaken mostly by the masonry arch ring which deforms more.

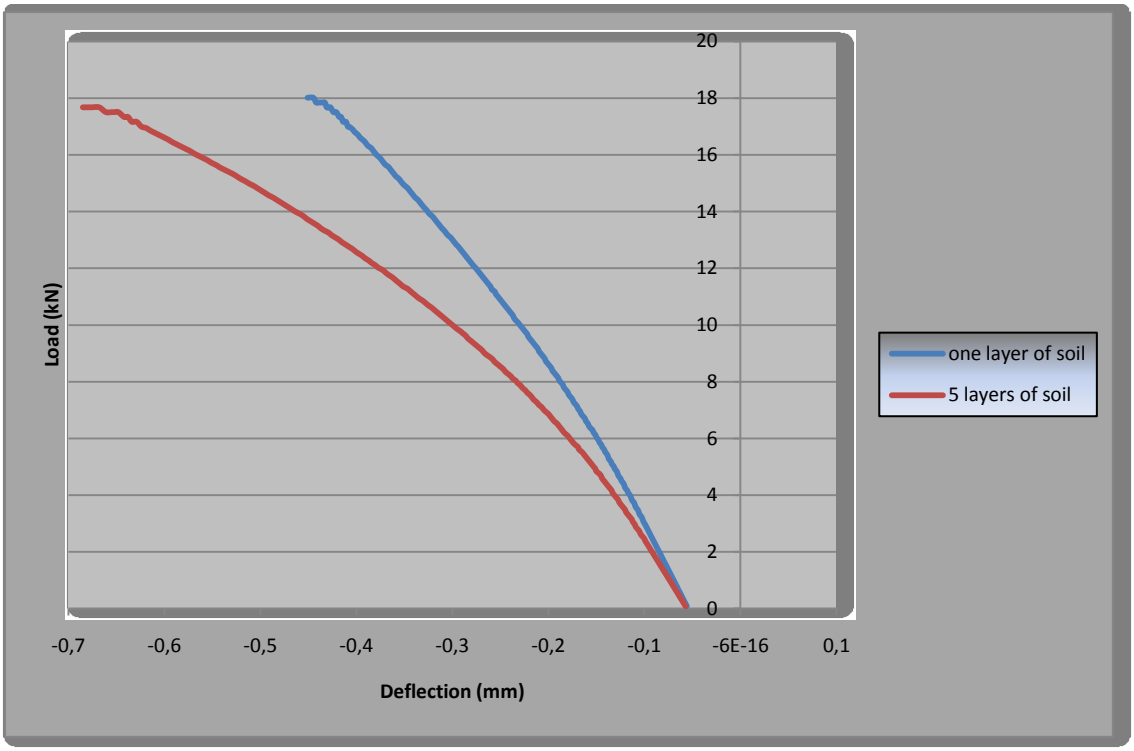

Figure 4- 34 Load-vertical displacement graph for one of the nodes on the intrados of the arch under the load application for model 2 and model 3

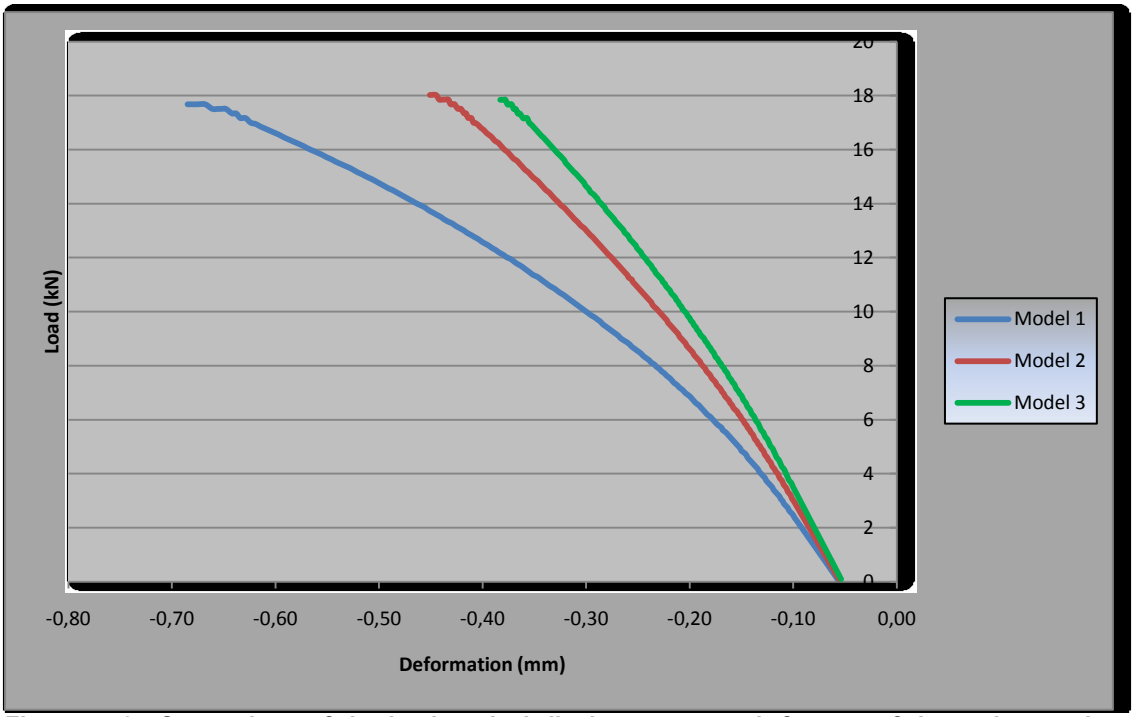

Figure 4- 35 Comparison of the load-vertical displacement graph for one of the nodes on the intrados of the arch for the three models

Figure 4-35 depicts the graphs load-vertical displacement for one of the nodes on the intrados of the arch for the three models. It is obvious that the stiffness of the model decreases in the case that the bracing system is simulated. It is also obvious that the stiffness decreases even more in the case that the soil is divided into several layers of different Young's modulus.

A comparison between the finite element analyses results and the results from the experimental procedure by means of magnitudes of displacements or loads would not make sense, since the assumptions made for the plane stress models lead to totally different results. The only comparison that can be done is of the shape, mainly the slope of the curve for each case.

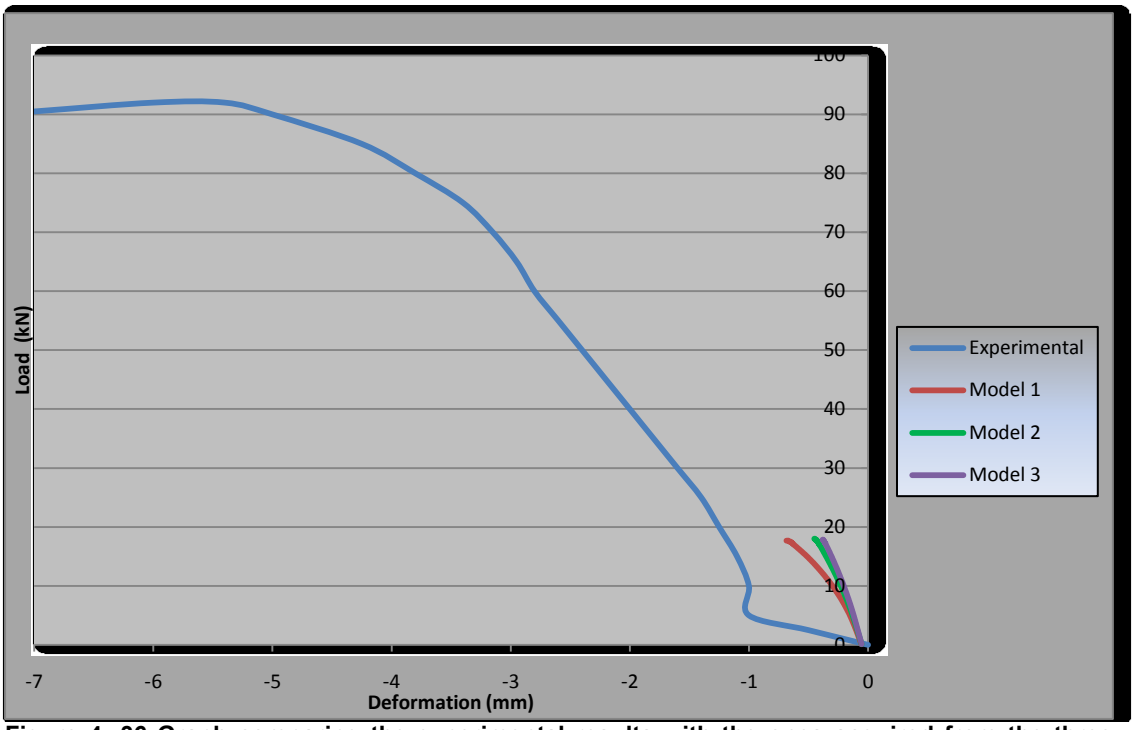

Figure 4- 36 Graph comparing the experimental results with the ones acquired from the three different models

In figure 4-36 we can see the comparison between the graphs load-deflection resulted from the finite element analyses and the one resulted experimentally. We can see that the stiffness of models 1 and 2 is bigger than the stiffness of the real structure. In opposite the stiffness of model 3 is smaller than the real one something expected from a plane stress model which does not take into account the contribution of the stiffness of the spandrel walls.

Also, in figure 3-25 which shows the graph load-deflection under the point of load application, we can distinguish a linear part in the beginning and thereafter the graph becomes non linear. Close to the ultimate load, there is a part of the curve for which the deflection is approximately constant. All these areas can be distinguished also in the corresponding graphs from the finite element analyses.

Furthermore, figure 3-25 presents only positive values that indicate descending of the point under consideration. In the graphs from the analyses for the same point we can see only negative values that also in this case indicate descending of this point (the Y axis is pointing upwards).

Also in figure 3-26 which shows the graph load-deflection at a point symmetrical to the point of load application we can see that in the beginning the values are positive (descending of the

point) and afterwards, the values become negative (rising of the point). Similar areas we can distinguish in figures 4-12(b), 4-18(b) and 4.27 which depict the graph load-deflection at a point symmetrical to the point of load application for each of the three analyses(in this case positive values indicate rising and negative values indicate descending).

5. THREE DIMENSIONAL FINITE ELEMENT MODEL ANALYSIS

5.1 Introduction

After the limit analysis and the finite element analysis of the plane stress model, the last step to be done is the finite element analysis of the 3D model. This kind of analysis is the most complex and time-consuming, but after the plane stress analysis we had already decided on the material properties to be used.

Once again we first ran a linear analysis in order to confirm that the model was working properly, but since such a model is not realistic and can not provide all the needed information about the ultimate load and the collapse mechanism, it was necessary to perform also a nonlinear analysis. Unfortunately, because of time limitations, a nonlinear analysis was not performed. As before, the FEM calculations were carried out by the FE program DIANA 9.4 which provides all the necessary non-linear constitutive models for the materials.

5.2 Basic assumptions

Given the fact that a three dimensional model of such a structure is very time-consuming and since the bridge is symmetric, we decided to model half of the structure and use symmetry constrains. Thus, the load applied on the structure, was half the ultimate load expected. In other words, we applied 46kN instead of 92kN. The load was applied only on the filling and not on the spandrel walls. Once again, for the application of the load we created a concrete beam on top of the filling and at ¼ of the arch span with dimensions 200mm*200mm*360mm. The load was applied as pressure distributed on the upper surface of this beam.

Moreover, the bridge was supposed to be fixed-ended under the concrete slabs and the x displacement was constrained in the right and left side of the structure, since the bracing system was not simulated.

Friction interface elements were introduced between the arch ring and the filling as well as between the spandrel wall and the filling in order to simulate possible relative slipping between the two.

We have to mention also that given the complexity of this model and the limitations of time, we had to divide the soil infill into two and not five layers.

5.3 Numerical modelling of the three dimensional configuration

Having the 2D geometry of the structure ready, the only thing that we had to do was to sweep it into several layers in order to create the volumes. The first layer was the spandrel wall, the second was the interface layer between the wall and the infill and the last one was the layer of the filling. The units used were: mm, N and kg.

Next we continued with the meshing of the model. The regular solid elements and the interface elements used for the meshing are listed and described below:

- **Solid element HX24L:** The HX24L element [Figure 5-1] is an eight-node isoparametric solid brick element. It is based on linear interpolation and Gauss integration.

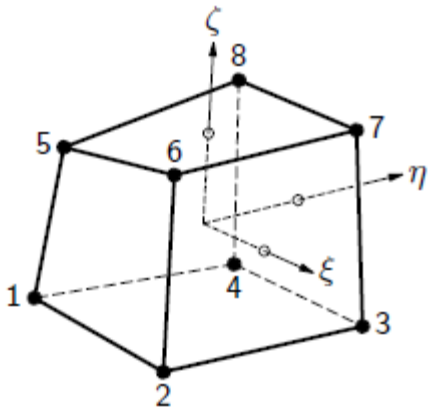

Figure 5- 1 HX24L

- **Solid elements TP18L:** The TP18L element [Figure 5-2] is a six-node isoparametric solid wedge element. It is based on linear area interpolation in the triangular domain and a linear isoparametric interpolation in the ζ direction.

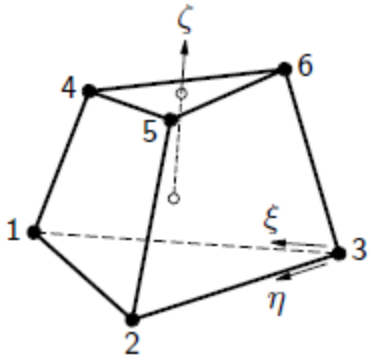

Figure 5- 2 TP18L

This element was only used on bodies which are consisted of triangular surfaces.

- **Interface element Q24IF:** The Q24IF element is an interface element between two planes in a three-dimensional configuration [Figure 5-3]. The element is based on linear interpolation.

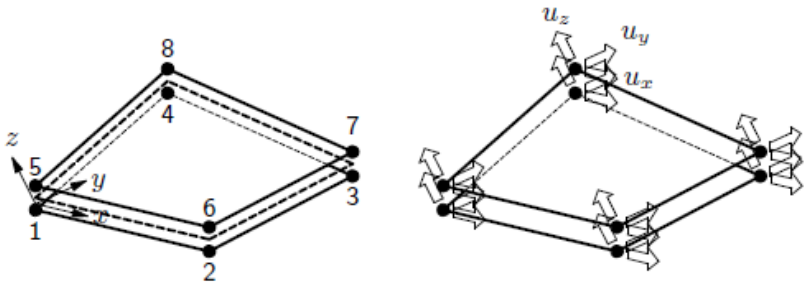

Figure 5- 3 Topology and displacements of Q24IF

- **Interface element T18IF:** The T18IF element is an interface element between two planes in a three-dimensional configuration [Figure 5.4]. The element is based on linear interpolation.

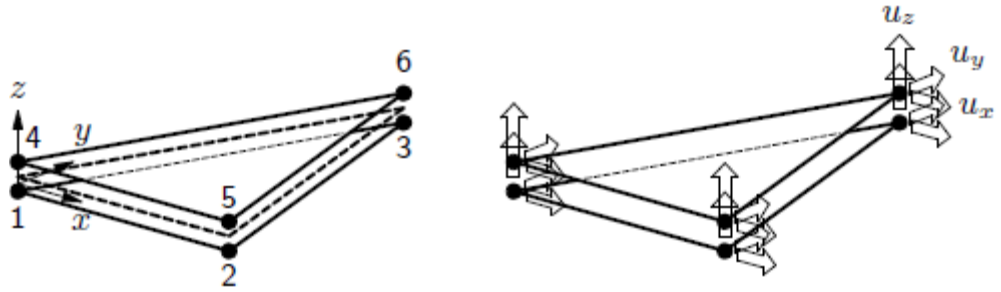

Figure 5- 4 Topology and displacements of T18IF

The mesh configuration is shown in figure 5-5. It has to be mentioned that the mesh on the ring is denser near the intrados and the extrados in order to avoid stress concentration at the points where the hinges are to be formatted.

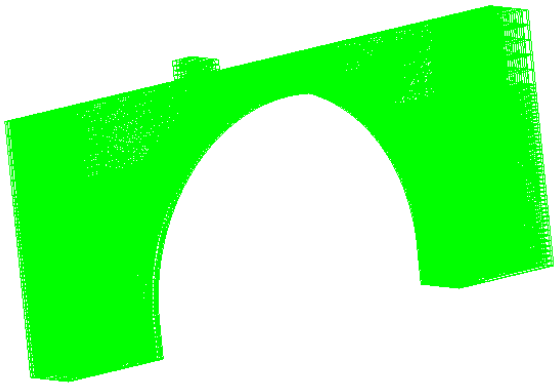

Figure 5- 5 Mesh configuration

The mesh includes 49430 nodes and 38480 elements. This means that since we have three degrees of freedom for each node for solid elements, the number of degrees of freedom in total is148290.

	Element type			
	HX24L	Q24IF	T81IF	TP18L
Number of elements	32564	5466	50	400

Table 5- 1 Number of elements for each element type

In table 5-1 we can see the number of elements for each of the element types used.

After the mesh generation, we defined the material properties as they are described in the next section. The material distribution on the model is shown in Figure 5-6. The final step was the definition of the constraints as explained before (fixed under the concrete slabs, constrain the x displacement on the right and left side of the bridge and symmetry constraints) and the application of the loads (self-weight and pressure on upper surface of the concrete beam).

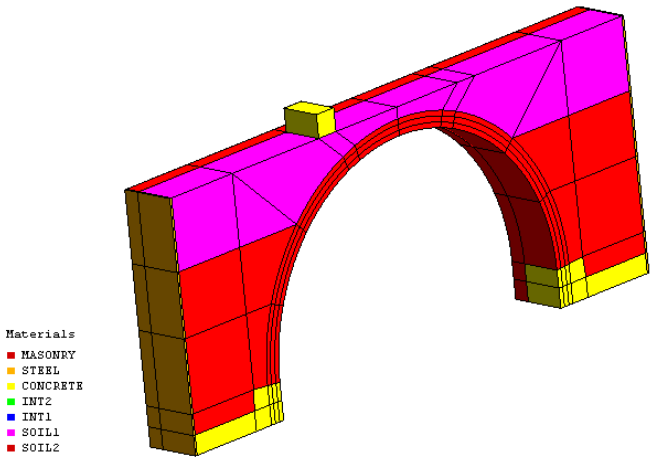

Figure 5- 6 The distribution of the different materials over the bridge

5.4 Linear analysis

The material properties used for the linear analysis are listed in the table below. We have to stress out the fact that interfaces were used not only between the masonry arch ring and the filling, but also between the spandrel wall and the filling.

Property	Concrete	Masonry	Soil (Layer 1)	Soil (Layer 2)	Interfaces
Young's Modulus	34000 N/mm^2	5500 N/mm^2	9.93 N/mm^2	28.81 N/mm^2	—
Poisson's ratio	0.15	0.18	0.2	0.2	—
Mass density	2.4e-06 kg/mm^3	1.8e-06 kg/mm^3	1.8e-06 kg/mm^3	1.8e-06 kg/mm^3	—
Linear normal stiffness	—	—	—	—	1e+06 N/mm
Linear tangential stiffness	—	—	—	—	1e+06 N/mm

Table 5- 2 Material properties for the linear analysis

The total load applied on the upper surface of the concrete beam was 46kN. The next pictures depict the results of the analysis.

The deformations of the whole structure are shown in Figure 5-7. The maximum deformation is located under the concrete beam ant it is 1.3cm. From this figure it is obvious that the spandrel wall's deformation is negligible in comparison with the deformation of the filling, since it is much stiffer and also the load is applied only on the filling.

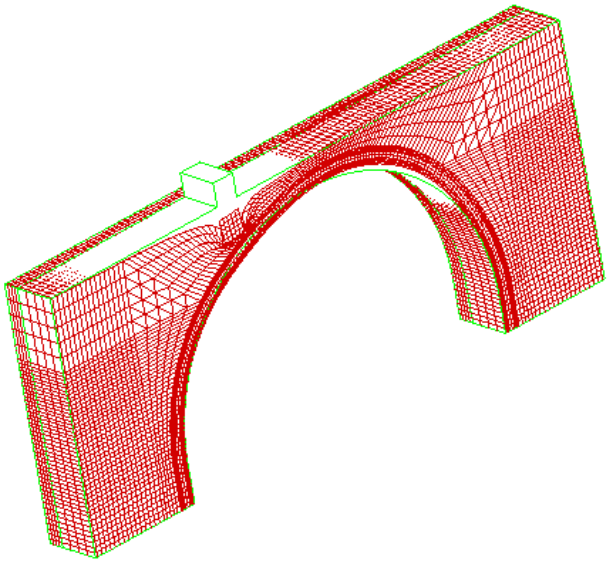

Figure 5- 7 Deformation of the bridge

In Figure 5-8 we can see the deformed shape of the arch barrel. The maximum deformation is 2.43mm and it is located on the intrados of the arch under the point of the load application and close to the spandrel wall. In this analysis, the maximum displacement of this point is much closer to the experimental results. We remind that the maximum displacement measured during the test on this point was approximately 5.5mm (Figure 3-25). Also the displacement on the extrados symmetrically to the point of load application is 2.28mm according to the finite element analysis and approximately 2.5mm according to the experimental results (Figure 3-27).

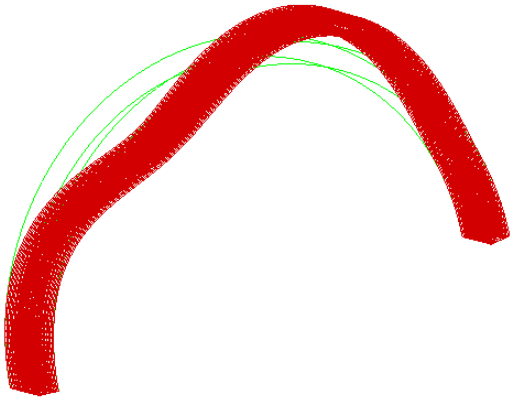

Figure 5- 8 Deformed shape of the arch barrel

From the above mentioned, we can conclude that the stiffness of the three dimensional model (we have maximum displacement 2.43mm) is bigger than the actual stiffness of the real structure (maximum displacement 5.5mm). This is coherent since we substituted the bracing system for constraints of the correspondent displacement and also divided the soil into only two layers, something that leads to a stiffer model as was proved by the different plane stress models.

Finally in figure 5-9 we can see the normal deformation of the spandrel wall. The maximum normal deformation is located on the crown and the relative displacement between the spandrel wall and the filling in the same location is 0.899e-2mm. Even though the magnitude is very small, it means detachment of the spandrel wall, something that actually happened during the experimental procedure.

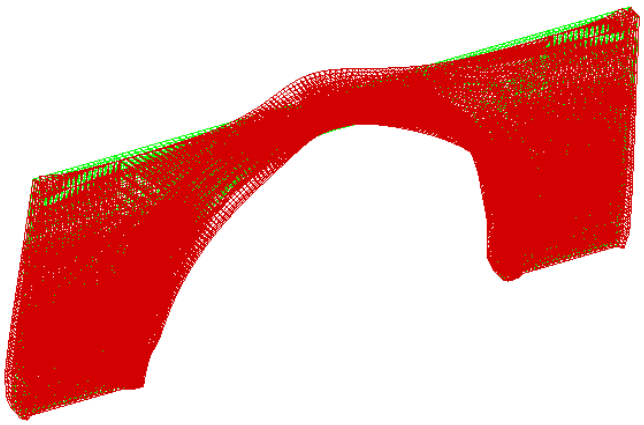

Figure 5- 9 Normal deformation of the spandrel wall

The next Figures depict the maximum principal strains on the whole bridge and on the arch barrel. In figure 5-11 we can see that the tensile strains are located on the areas where the hinges are expected to appear.

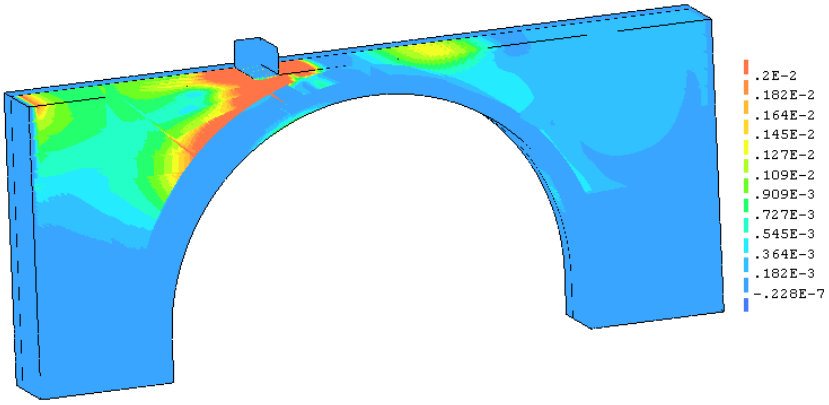

Figure 5- 10 Maximum principal strains on the bridge (P_{1max}=0.0135mm/mm, P_{1min}=-.228e-7mm/mm).

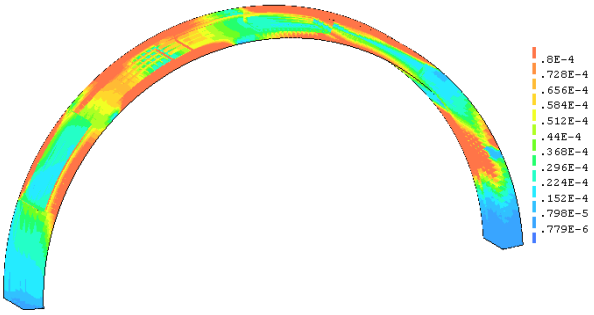

Figure 5- 11 Maximum principal strains on the arch ring (P_{1max}=0.827e-3 mm/mm, P_{1min}=0.779e-6 mm/mm).

Finally on Figures 5-12, 5-13, 5-14 and 5-15 we present the maximum and minimum principal stresses on the bridge and on the arch ring. It is clear that the maximum and the minimum principal stresses are concentrated on the arch ring rather than the rest of the structure. We can also see in figure 5-12 that areas close to the expected hinges have overcome the tensile strength of the masonry.

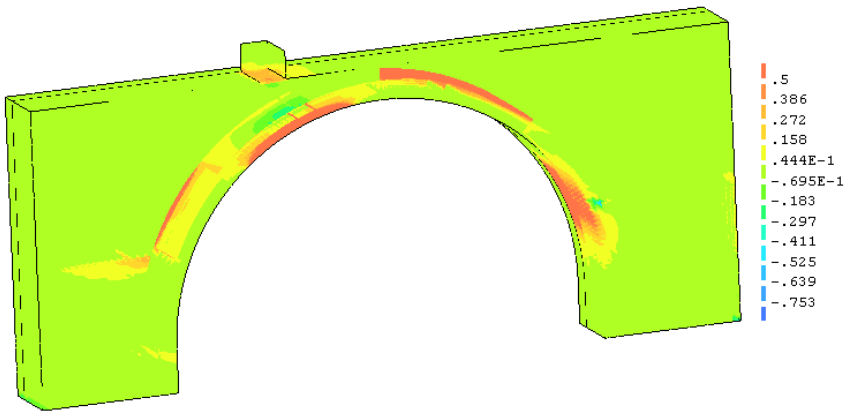

Figure 5- 12 Maximum principal stresses calculated from s_{xx} (P_{1max}=4.58MPa, P_{1min}=-0.753 MPa)

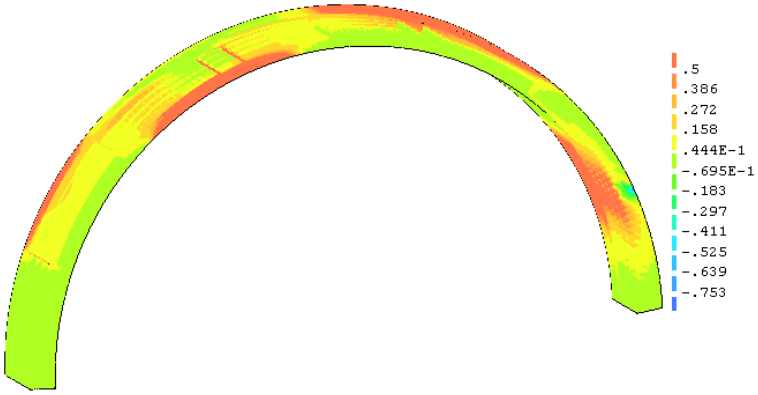

Figure 5- 13 Maximum principal stresses calculated from s_{xx} (P_{1max}=4.58MPa, P_{1min}=-0.753 MPa)

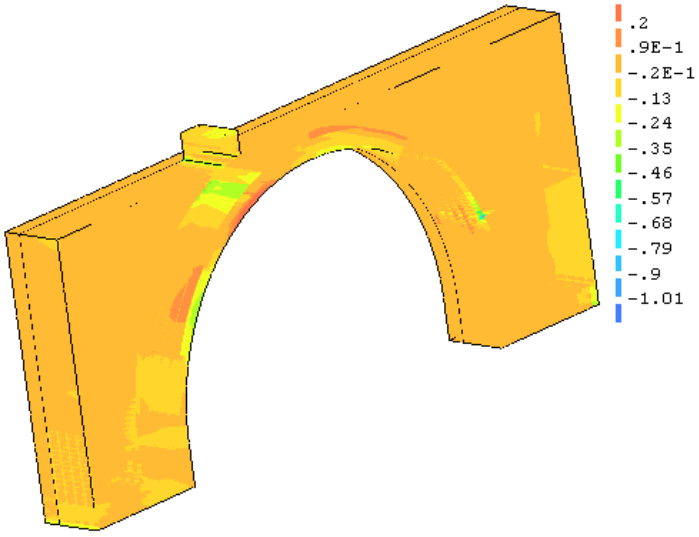

Figure 5- 14 Minimum principal stresses calculated from s_{xx} (P_{2max}=0.441 MPa, P_{1min}=-1.01 MPa)

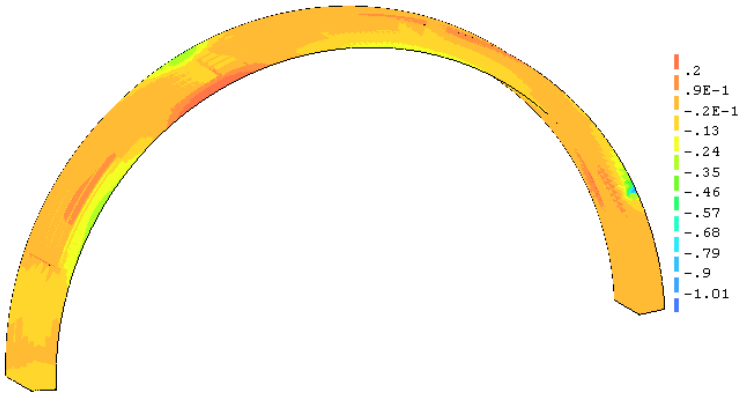

Figure 5- 15 Minimum principal stresses calculated from s_{xx} (P_{2max}=0.441 MPa, P_{1min}=-1.01 MPa)

Except the basic conclusions mentioned before, a linear analysis can not lead to more specific and realistic conclusions about the actual ultimate load or about the collapse mechanism. For that, it is necessary to perform a nonlinear analysis.

6. CONCLUSIONS

Before proceeding to a finite element analysis it is very important to be aware of the exact experimental procedure. More specifically, it is necessary to know the materials used, the constraints, the condition of loading and most important the results achieved in order to calibrate the model.

Moreover, a limit analysis is a very helpful tool, since it gives a first impression about the ultimate load and the collapse mechanism. Also running a number of limit analyses by differentiating the properties of the materials helps to understand the way that each parameter influences the behavior of the structure.

Summarizing chapter 4, three different finite element models were examined and lead to some conclusions regarding the way that the structure works and the importance of selecting the appropriate material properties during an analysis. The most important of these conclusions are discussed in section 6.1.

Finally, in section 6.2 we present some basic conclusions about the linear analysis of the three dimensional finite element model. The results as well as the conclusions would be much more essential if we had the time to perform a nonlinear analysis on this model.

6.1 Conclusions on the plane stress model analyses

Firstly, we have to mention that before deciding to use the material properties presented in chapter 4, a number of analyses was performed by differentiating each time a different material property. The load carrying capacity of the finite element mode is very sensitive to the material properties such as density, cohesion of soil, the internal friction angle and dilatancy angle and the tensile strength of the brickwork. For example if we increase the cohesion of all the soil layers of model from 0.018 N/mm^2 to 0.02 N/mm^2 the ultimate load is increased from 17.68kN to 19.72kN.

Also before reaching to the mesh configuration that we presented, we had created a more coarse mesh. The mesh was coarser with only 4 elements along the width of the arch ring. In this case it was difficult to achieve convergence. So the mesh of the width of the arch ring has to be dense to achieve the right distribution of stresses.

Moreover, the simulation of the actual bracing system that was used during the experimental procedure instead of substituting it with constraints of the corresponding displacements, leads to more realistic results. It has to be reminded that in the analyses where the bracing system was simulated, the resulting ultimate load was closer to the one calculated by the limit analysis using RING 2.0. Also even thought that in model 2 the collapse mechanism was not fully formed, the position of the four plastic hinges was clear and in accordance with the limit analysis. Furthermore, the stiffness of the model was smaller compared to model 1,

approaching more the stiffness of the real structure. Nevertheless, the stiffness was not smaller than the real one as expected.

Finally, our initial assumption that the Young's modulus of the soil is not constant, but it is increasing with the depth was correct. This fact is clear from the results of the analysis of model 3 for which the soil filling was divided into five layers with different Young's modulus for each one. In this analysis, the ultimate load reached was very close to the one calculated from the limit analysis (17.68kN is the one calculated from the nonlinear finite element analysis and 16.528kN the one calculated from the limit analysis). Also in this case, the collapse mechanism of the four plastic hinges is fully formed and the hinges are positioned in areas that we expected (on the intrados of the arch under the load application, on the extrados of the arch symmetrically to the point of load application, on the extrados of the arch and near the left abutment and on the intrados of the arch close to the right abutment). Moreover the stiffness of this model is smaller than the stiffness of the previous models and also smaller than the one of the real structure. This is coherent since in this plane stress model the spandrel walls are disregarded and hence their contribution to the stiffness of the structure.

6.2 Conclusions on the three dimensional model analysis

Of course it is undeniable that a three dimensional model of such a complicated structure is more realistic and can lead to results very close to the ones achieved from the experiment. Also a properly developed 3D model could be used to predict the results of future full scale experiments on masonry arch bridges.

Despite, of course, of the advantages of such a model, there are also a lot of problems that a designer has to face while generating it. This is a very complicated and time consuming procedure, mostly due to the use of 3D interface elements to simulate the interface between the filling and the spandrel walls as well as the interface between the masonry arch barrel and the filling. This is the reason why we managed to perform only a linear analysis of the 3D model in the limited time to conduct this master thesis.

Even though the linear analysis presented in chapter 5 is not able to provide us the information needed about the ultimate load and the collapse mechanism of the bridge, it gave us some interesting initial information and also the hope that a nonlinear analysis will lead to the desirable results.

The displacements calculated from the finite element analysis (2.43mm displacement on the intrados of the arch under the point of load application), are close to the maximum displacements calculated during the experiment (5.5mm maximum displacement on the intrados of the arch under the point of load application). Also the spandrel wall has been detached from the soil infill on the crown, something that is in accordance with the

experimental procedure. Moreover the stiffness of the three dimensional finite element model, is bigger than the stiffness of the real structure since the bracing system was not simulated and the soil was divided into only two layers. This proves the importance of simulating the real boundary conditions of the structure. Finally the maximum principal strains and stresses on the arch are located on the areas where the four plastic hinges are expected to be generated.

6.3 Suggestions for further research

Of course the first thing to suggest for further study, is the performance of a nonlinear analysis on the 3D model which as mentioned before will lead to results close to the experimental ones. But except that, there are more things that could improve the results especially on the 3D model.

Firstly a 3D model with more soil could present a more realistic behavior of the structure. We have to remind that in the present thesis the 3D model created had only two layers of soil and it was proved by the plane stress model that the soil should be divided into many layers with different Young's modulus.

Moreover we used the Mohr-Coulomb constitutive model for the soil but the model that best describes such a material is the Modified Mohr-Coulomb constitutive model. So, a comparison between the results of the two models would be very interesting.

We have noted before the importance of simulating the bracing system. Thus, a 3D model with simulation of the actual bracing system (tubular profiles and not a steel plate of equivalent thickness) could help us to better understand the structure and the influence of the bracing system itself.

REFERENCES

Alexandre Rodriguez Castiblanque, Analisis experimental de la capacidad portante be un Puente arco de obra fabrica de ladrillo, UPC 2003.

P. Roca, C. Molins, Experiments on arch bridges, Arch Bridges ARCH´04, CIMNE, Barcelona, 2004.

P. Roca, C. Molins, A. C. Aparicio and V. Sarrablo, Laboratory experiments on the service and ultimate response of arches.

G. Frunzio, M. Monaco, 3D F.E.M. analysis of a Roman arch bridge, Historical Constructions, P.B. Lourenço, P. Roca (Eds.), Guimarães, 2001.

C. Molins, P. Roca, Capacity of masonry arches and spatial frames, Journal of structural engineering, 1998.

J. Wang, C. Melbourne, Finite element analyses of soil-structure interaction in masonry arch bridges, 5th International conference on arch bridges, 2007.

Maria Rota, Seismic vulnerability of masonry arch bridge walls, Rose school, 2004.